**M-AM-Tut** TUTORIAL: INSERTION OF PROTEINS INTO MEMBRANES.
Peter Walter, UCSF Medical Center, San Francisco, CA
Thomas Thompson, University of Virginia, Charlottesville, VA
Frederic Richards, Yale University, New Haven, CT
Adrian Parsegian, National Institutes of Health, Bethesda, MD.

This session has been designed to stimulate biophysical examination of phenomena that are more usually the concern of cell biologists. After synthesis, proteins can move into or across cell membranes. But still we can only guess what features of component lipids and peptides cause the many different observed forms of protein-lipid organization. Our aim is to present data in a way that creates practical questions susceptible to physical methods of thinking.

We begin with a review from the perspective of a molecular cell biologist (Walter) dealing specifically with translocation across the endoplasmic reticulum. Then several model and natural systems will be described (Thompson and Richards) that show protein incorporation and enforced removal. The formal presentation will end with a description and comparison (Parsegian) of the physical and chemical forces likely to be encountered in protein insertion and removal.

The speakers encourage audience response and will produce a set of questions to seed a general discussion.

**M-AM-A1** CHEMICAL COMPOSITION AND PHOTOCHEMICAL PROPERTIES OF REACTION CENTERS FROM THE PHOTOSYNTHETIC BACTERIUM CHLOROFLEXUS AURANTIACUS L. J. Mancino, P. L. Hansen, R. E. Stark and R. E. Blankenship, Dept. of Chemistry, Amherst College, Amherst, MA, 01002.

Reaction centers were prepared from the thermophilic green photosynthetic bacterium Chloroflexus aurantiacus using a procedure modified from that of Pierson and Thornber (PNAS 80, 80-84, 1983). SDS gel electrophoresis of the unheated reaction center complex gave a single band with apparent $M_r$ 52,000 which retained its native absorption spectrum and photoactivity. Reaction centers heated for 10 seconds at 85 C exhibited two electrophoretic bands with $M_r$ 27,000 and 29,000. Continued heating led to aggregation of the 29 kDa peptide, with no effect on the 27 kDa peptide. The amino acid composition indicates that the reaction center is only distantly related to that of the purple bacterium Rps. sphaeroides. Gel filtration on Sephacryl S-300 gave an apparent MW of 81 kDa, consistent with a complex composed of two peptides and bound detergent. Purified reaction centers have an isoelectric point of 6.45-6.8. Pigment analysis indicated that Chloroflexus reaction centers contain equal amounts of bacteriochlorophyll and bacteriopheophytin. An experiment in which the optical absorbance and the ferricyanide-induced $P870^+$ ESR signal were compared gave an absolute pigment composition of 3 BChl and 3 BPh and an extinction coefficient of 184 $mM^{-1}cm^{-1}$ at 812 nm. Atomic absorption analysis indicated that Chloroflexus reaction centers contain no Fe and approximately one Mn per center. Binary oscillations of absorption at 450 nm indicative of a functional two-quinone acceptor system were observed. The electron transfer from $Q_A^-$ to $Q_B$ was found to be sensitive to the inhibitor o-phenanthroline but not to the herbicides atrazine and terbutryn.

**M-AM-A2** PURIFICATION, PHYSICAL PROPERTIES AND KINETIC BEHAVIOR OF CYTOCHROME c554 FROM CHLOROFLEXUS AURANTIACUS R. E. Blankenship, P. Huynh, H. Gabrielson and L. J. Mancino, Dept. of Chemistry, Amherst College, Amherst, MA, 01002.

The membrane-bound cytochrome c-554 that serves as electron donor to $P870^+$ in the thermophilic green photosynthetic bacterium Chloroflexus aurantiacus (Bruce et al. PNAS 79 6532-6536, 1982) has been purified and characterized. After detergent-induced release from the cytoplasmic membrane and purification using DEAE Sephacel, the cytochrome is soluble in the absence of added detergent. Gel filtration on Sephacryl S-300 yields an apparent $M_r$ 440,000, implying that large aggregates are present in solution. SDS gel electrophoresis gives a single band with $M_r$ 43,000. Heme-stained gels of membranes show 3 peptides with $M_r$ 79,000, 43,000 and 25,000. The pI of the purified cytochrome is 6.1. Cytochrome c-554 contains two spectrally identical but thermodynamically distinct hemes, with midpoint redox potentials of +140 and +265 mv at pH 8. Pyridine hemochrome and Lowry protein assays and atomic absorption analysis also indicate 2 hemes per peptide. The extinction coefficient at 554 nm is 26.2 $mM^{-1}cm^{-1}$. Kinetic experiments indicate that the purified cytochrome is photooxidized only very slowly by either Rps. sphaeroides R-26 or Chloroflexus reaction centers. Horse heart cytochrome c is readily photooxidized by Rps. sphaeroides but only very slowly photooxidized by Chloroflexus reaction centers. The interaction between the cytochrome and the reaction center of Chloroflexus is apparently somewhat different from the electrostatic attraction usually found between soluble c-type cytochromes and their oxidases.

**M-AM-A3** ORIENTATION OF CYTOCHROMES C AND $C_2$ IN THE ELECTRON TRANSFER COMPLEX FORMED WITH Rps. sphaeroides REACTION CENTERS AND BOUND TO THE MEMBRANE SURFACE. David M. Tiede[1,2] and Jacques Breton[1], 1) Service de Biophysique, C.E.N. de Saclay, 91191 Gif-sur-Yvette, France 2) Present Address: Chemistry Division, Argonne National Laboratory, Argonne, Il. 60439

Previous spectroscopic studies have shown that the electron tunneling within the bacterial reaction center (RC) and with the associated c-hemes in C. vinosum and Rps. viridis, occur through geometries in which the redox groups are oriented in a non-coplanar fashion. Here, we examined the orientations of cyt c and $c_2$ in transient complexes bound to 1) their oxidation site on the Rps. sphaeroides RC and 2) to sites at the membrane surface. The oxidation of cyt c/$c_2$ has biphasic kinetics. Flash-induced dichroism measurements with RC-phosphatidylcholine reconstituted vesicles ordered in squeezed acrylamide gels, show that only the fast phase of cyt c/$c_2$ oxidation is dichroic, corresponding to a tilt of the heme normals of 20°-30° away from the membrane normal. The dichroism spectra for the c and $c_2$ are different, possibly indicating that cyt $c_2$ is inclined more towards the membrane normal. The slow phase of cyt c/$c_2$ oxidation is non-dichroic, which may arise as a result of a faster rotational motion. Linear dichroism spectra of cyt c/$c_2$ bound to RC vesicles show a dichroic binding site stoichiometry of (0.5 cyt c/$c_2$)/RC. Although the bacteriochlorophyll dimer cation (the oxidant of the cyt c/$c_2$ hemes) is similarly tilted at 10°-20° away from the membrane normal, photoselection experiments indicate that in the cyt c/$c_2$-RC complex, these groups are not aligned in a co-planar manner. The orientation of cyt c/$c_2$ bound to the RC protein is analogous to its orientation when bound to the surface of negatively charged, lipid membranes.

**M-AM-A4** RECONSTITUTION OF IRON-DEPLETED REACTION CENTERS FROM RHODOPSEUDOMONAS SPHAEROIDES R-26 WITH Fe, Mn, Cu, & Zn.* R. J. Debus, M. Y. Okamura, and G. Feher; U.C.S.D., La Jolla, CA 92093.

Reaction Centers from R. sphaeroides R-26 were depleted of Fe by incubation with 1.5M LiSCN and 1 mM o-phenanthroline in the presence of 0.03% Na cholate at 4°C (pH=8). The resulting RCs contained <0.1 Fe/RC as determined by atomic absorption. The rates of electron transfer from $Q_A^-$ to $Q_B^-$ ($k_{AB}$), $Q_B^-$ to $D^+$ ($k_{BD}$), and $Q_A^-$ to $D^+$ ($k_{AD}$) were slower in Fe-depleted RCs compared to native RCs. Incubation of Fe-depleted RCs with $Fe^{2+}$, $Mn^{2+}$, $Cu^{2+}$, and $Zn^{2+}$ restored these rates to values close to those found in native RCs. These findings suggest that Fe, Mn, Cu, and Zn were incorporated into the Fe-binding site of the Fe-depleted RCs and that removal of the Fe caused a reversible conformational change in the RC. These results provide further confirmation that Fe is not required for rapid electron transfer from $Q_A^-$ to $Q_B$ (1,2).

| RC sample | $k_{AB}$ [$10^3$ $sec^{-1}$] | $k_{BD}$ [$sec^{-1}$] ± 0.05 | $k_{AD}$ [$sec^{-1}$] ± 0.5 |
|---|---|---|---|
| Native | 5.0 ± 0.2 | 0.66 | 8.3 |
| Fe-depleted | 1.5 ± 0.5 | 0.20 | 5.2 |
| + Fe | 4.9 ± 0.3 | 0.62 | 8.1 |
| + Mn | 5.4 ± 0.3 | 0.68 | 8.0 |
| + Cu | 5.2 ± 0.2 | 0.42 | 9.0 |
| + Zn | 6.0 ± 0.4 | 0.81 | 7.7 |

*Work supported by grants from NSF and NIH.

(1) R. J. Debus, M. Y. Okamura, and G. Feher (1984) Biophys. J. 45, 255a.
(2) H. K. Nam, R. H. Austin, and G. C. Dismukes (1984) Biochim. Biophys. Acta 765, 301-308.

**M-AM-A5** ENDOR OF UBISEMIQUINONE IN REACTION CENTERS FROM R. SPHAEROIDES IN WHICH Fe WAS REPLACED BY Zn.* W. Lubitz, R. J. Debus, M. Y. Okamura, & G. Feher, U.C.S.D., La Jolla, CA 92093.

Ubiquinone radicals were prepared in iron-depleted Reaction Centers (RCs) reconstituted with Zn (1) (EPR linewidth 8.0 G, g=2.0046). The primary quinone radical $Q_A^-$ was generated by illumination in the presence of cytochrome c. Its X-band ENDOR spectrum (first derivative) at -150°C is shown in the figure. The following hyperfine coupling constants were resolved: $A_1$ = 0.5, $A_2$ = 1.1, $A_3$ = 2.5, $A_4$ = 4.1, $A_5$ = 4.6, $A_6$ = 6.5 MHz. Some of these correspond approximately to the values observed in the iron-depleted LM complex (2). The region close to the free proton frequency (3) may contain information about interactions with the protein environment. The radical of the secondary quinone $Q_B^-$, prepared by a single laser flash, showed differences in the ENDOR spectrum, probably reflecting a change in its surrounding.

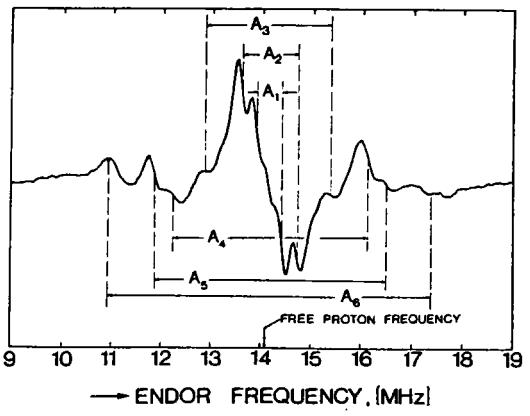


*Supported by grants from NIH, NSF & M. Kade Fdn. (W.L.).

(1) R. J. Debus, et al, see preceding abstract.
(2) M. Y. Okamura, et al, Fed. Proc. 39, 1802 (1980).
(3) P. J. O'Malley & G. T. Babcock, J. Chem. Phys. 80, 3912 (1984).

**M-AM-A6** HYBRIDIZATION OF RC SUBUNITS FROM NATIVE AND HERBICIDE RESISTANT STRAINS OF RHODOPSEUDOMONAS SPHAEROIDES - LOCALIZATION OF THE HERBICIDE BINDING SITE.* M. Y. Okamura, E. C. Abresch, R. J. Debus, and G. Feher, U.C.S.D., La Jolla, CA 92093.

Reaction centers were isolated (1) from triazine resistant strains of R. sphaeroides. These RCs exhibit a decreased sensitivity to herbicide and a low rate of light-induced electron transfer using cytochrome c as a donor and $UQ_o$ as the acceptor. The mutant RCs were hybridized with either LM or H subunits from native RCs by treatment with 0.75 M $LiClO_4$ (2). In three mutants investigated, LM restored rapid electron transfer, while H did not. This assay indicates that the mutation site is on the LM unit. This finding is in agreement with results obtained from more specific localization experiments (3,4). It is, however, conceivable that the H-subunit may be involved in other mutations. The advantage of the hybridization experiments is the simplicity and ease with which a large number of mutants can be screened.

*Work supported by the USDA.

(1) Okamura, M. Y. (1984) in Biosynthesis of the Photosynthetic Apparatus (R. Hallick, L. A. Staehlin, and P. J. Thornber, eds.), pp. 381-390, Alan Liss, N. Y.
(2) Debus, R. J., Feher, G., and Okamura, M. Y. (1984) Biochemistry, submitted.
(3) de Vitry, C., and Diner, B. A. (1984) FEBS Letters 167, 327-333.
(4) Brown, A. E., Gilbert, C. W., Guy, R. and Arntzen, C. J. (1984) PNAS, submitted.

**M-AM-A7** RAPID OXIDATION OF REDUCED PRIMARY ACCEPTOR QUINONE IN Rp. viridis REACTION CENTERS BY FERRICYANIDE R.J. SHOPES and C.A. WRAIGHT, U. of ILLINOIS, URBANA

Illumination of photosynthetic reaction centers from Rp. viridis containing a single quinone, poised at $E_h$ = +440mV with ferricyanide, induces the charge separated state $P^+ Q_A^-$. Contrary to expectation the decay of $P^+$, the oxidized donor, was biphasic - a result of competition between the direct charge recombination (fast) and an indirect pathway, the oxidation of $Q_A^-$ by ferricyanide followed by slow reduction of $P^+$ by ferrocyanide. Oxidation of $Q_A^-$ by ferricyanide was much faster for a protonated state of the reaction center, as was the reduction of $P^+$ by ferrocyanide. However, it could not be determined if these rates were controlled by the same protonatable group. Thus, in the scheme below, $pK_1$ is not necessarily equal to $pK_5$ even though the donor and the acceptor are in the same state in both cases (similarly for $pK_3$ and $pK_4$).

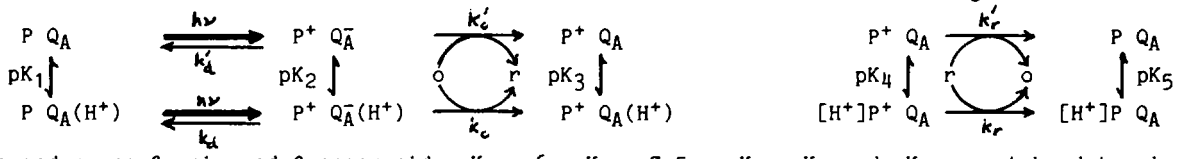


o and r are ferri- and ferrocyanide $pK_2$ ~ 6; $pK_4$ ~ 7.5. $pK_1$, $pK_3$ and $pK_5$ cannot be determined by these kinetic measurements. In 0.1M NaCl, $k_o$ ~ $10^8$, $k_o'$ ~ $10^5$, $k_r$ ~ $10^5$ and $k_r'$ ~ $10^3$ (all $M^{-1}s^{-1}$); the direct recombination rates are $k_d$ = $1.5x10^3 s^{-1}$ and $k_d'$ = $0.8x10^3 s^{-1}$. These results imply a surprising accessibility of $Q_A^-$ to a highly charged species. Supported by NSF PCM 83-16487.

**M-AM-A8** CRYSTALLIZATION OF AN ANTENNA PIGMENT-PROTEIN COMPLEX FROM RHODOPSEUDOMONAS SPHAEROIDES.* J. P. Allen, R. Theiler, and G. Feher, U.C.S.D., La Jolla, CA 92093.

The B800-850 antenna complex from R. sphaeroides 2.4.1 was solubilized with β-D-octyl glucopyranoside and purified by column chromatography on DEAE-cellulose in the presence of nonanoyl-N-methylglucamide. The purified complex was essentially free of contaminating pigment-protein complexes and showed an A800/A850 ratio of 0.63. For crystallization the nonanoyl-glucamide was exchanged against β-octyl glucoside by dialysis. The crystallization procedure combined the methods that have recently been developed for integral membrane proteins (1,2,3). The solution of protein ($A_{1\,cm}^{845}$ = 18), 0.3M NaCl, 9% polyethylene glycol 4000 (PEG), and 1,2,3-heptane triol was slowly equilibrated by vapor diffusion against 25% PEG and 0.8 M NaCl. Crystallization proceeded at room temperature in the dark. After two weeks, diamond-shaped micro-crystals were observed, having dimensions of ∿ 0.1 mm (long axis)(see figure). The crystals were birefringent and exhibited the characteristic absorption bands of the antenna pigment-protein complex in solution.

*Work supported by grants from the NIH and the NSF.

(1) R. M. Garavito, J. Jenkins, J. N. Jansonius, R. Karlsson, and J. P. Rosenbush (1983) J. Mol. Biol. 164, 313.
(2) H. Michel (1982) J. Mol. Biol. 158, 567.
(3) J. P. Allen and G. Feher (1984) PNAS 81, 4795.

**M-AM-A9** ELECTRIC FIELD DEPENDENCE OF RECOMBINATION KINETICS OF PHOTOSYNTHETIC REACTION CENTERS IN LANGMUIR-BLODGETT FILMS. G.Alegria, P.L.Dutton, U. Of PA. Phila.PA19104. Z.Popovic, G.J.Kovacs, Xerox Res. Centre of Canada. Mississauga Ont. L5K 2L1.

The kinetics of charge recombination of Langmuir-Blodgett (LB) films of reaction centers (RCs) from Rps. sphaeroides. were measured after a saturating xenon flash as a function of an externally applied field.LB films of RC preparations with 90% single quinone (1Q/RC),80% two quinone (2Q/RC) as well as films of 1 Cl anthroquinone and duroquinone reconstituted RCs were tested.The films were formed on an air-water interface and deposited onto conductive quartz slides.After 2-4 layers were deposited the films were coated with a blocking polymer and a second electrode (In or Al) was evaporated on top.Electric fields up to 160V/μm were applied and absorption changes at 862nm measured. Kinetics of charge recombination at each step of the sandwich making process were measured to check the integrity of the RCs.The transference of the RCs to a "dry state" produced changes in the kinetics.Layering of blocking polymer and electrode evaporation did not introduce major changes.From 30% to 50% of the RCs were still active at the end.The absorption recovery at zero field was fitted with 3 exponentials and the field dependence of the rates was obtained using a new deconvoluting technique.For all the films tested the first two rates closely follow an exponential function of the field.Five-fold changes of the rates were observed at max. field.Native RC films showed asymmetric "up" and "down" populations and photoinduced electric transients were measured.From the sign of the electric signal it was determined that an increase of the energy gap between charge separated and ground states increases the decay rate. Action spectra of the light induced voltage are very similar to optical spectra of RCs in solution.

**M-AM-A10** PICOSECOND TRANSIENT OPTICAL ABSORBANCE MEASUREMENTS ON SINGLE CRYSTALS OF THE REACTION CENTER PROTEIN FROM R. viridis. M. R. Wasielewski, R. Gerald and P. Gast, Chemistry Division, Argonne National Laboratory, Argonne, IL 60439

Single crystals of the reaction center protein from R. viridis were grown using the method of Michel. Small, optically thin crystals were selected for study. The crystals were placed in a buffer containing ascorbate to keep the attendant cytochromes reduced. The crystals were mounted in flat double capillaries. A picosecond laser which produced 2 psec pulses at either 610 nm or at 947 nm by raman shifting was used as the excitation source. Part of the picosecond laser pulse energy was used to generate a 2 psec broadband white light probe pulse. A 1000x microscope was incorporated into the double beam picosecond absorbance spectrometer. This allowed detection of only that probe light which passed through the approximately .01 mm x .003 mm x .003 mm single crystal. About 5-10 microjoules of laser light was used to excite the crystal. Transient absorption changes were measured as a function of time, wavelength, and orientation of the polarized excitation beam relative to the crystal axes. The transient absorbance of primary radical pair state $P^F$ was found to depend strongly on the orientation of the electric field vector of the laser excitation pulse relative to the crystal axes. The results will be discussed in terms of the seemingly redundant electron transport chromophores in the reaction center. (This work was supported by the Division of Chemical Sciences, Office of Basic Energy Sciences, U.S. Department of Energy under contract W-31-109-ENG-38.)

**M-AM-A11** FIRST FLASH PROTON BINDING BY THE ACCEPTOR QUINONE COMPLEX OF REACTION CENTERS FROM Rp. sphaeroides. P. MARÓTI AND C. WRAIGHT, University of Illinois, Urbana.

Rapid (ms) $H^+$ binding after a single flash was measured by two independent techniques: optically by pH indicator dyes (see figure) and electrically by conductance changes. The two methods gave a similar pH dependency: very low $H^+$ uptake at low pH(<8), increasing to a maximum at pH=9-10. The decline in $H^+$ binding at high pH was associated with the redox-pK of the quinone species involved - $Q_A^-$ or $Q_B^-$. The pK for $Q_A^-$ was shifted in the presence of terbutryn.

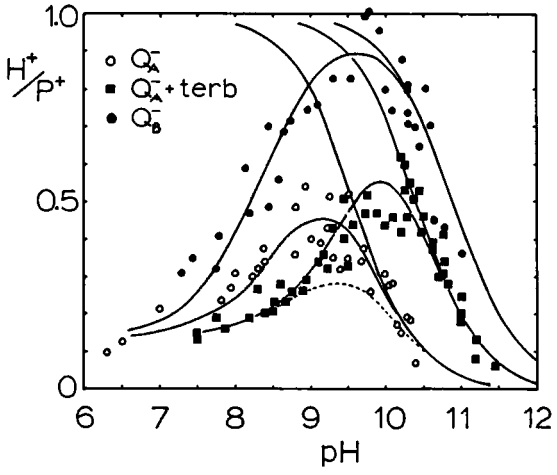


Equilibrium redox titrations of $Q_A/Q_A^-$ demonstrated the expected pKs for $Q_A^-/Q_A^-(H^+)$, but predict maximal $H^+$ binding at all pHs below the pK region. Thus, the failure to observe $H^+$ binding indicates a kinetic block, active on the seconds time scale. Preliminary data show slow proton binding at low pH in the minutes time range which supports the non-equilibrium character of the fast $H^+$ binding.

Supported by NSF PCM 83-16487.

**M-AM-B1** Immunologically Active Metal Substrates*, J. A. Panitz, Sandia National Laboratories, Albuquerque, NM 87185.

The formation of immunologic multilayers on metal substrates is being studied by a novel transmission electron microscope imaging technique. Layer morphology is observed in a direction normal to the substrate surface, at a resolution of about 1 nm. Direct visualization of antigenic monolayers of horse spleen ferritin and bovine serum albumin is being used to probe seocnd and third layer formation by the immune reaction, using polyclonal and monoclonal IgG. Antibody layer morphology, non-specific binding of IgG, and passivation of the metallic substrate by small protein adsorbates is being investigated. Examples will be presented that support a new solid state chemical sensor concept in which an immunologically active diode, operating in a liquid environment, is envisioned.
*This work supported by the Defense Advanced Research Projects Agency under ARPA contract # 4597.

**M-AM-B2** ENERGY-FILTERED IMAGES OF URANIUM AND CARBON IN NEGATIVELY STAINED CATALASE. C.-F Chang H. Shuman and A.P. Somlyo. Penn. Muscle Inst., U. of Penn. Phila., PA 19104.

Energy-filtered electron microscopy with a spectrometer attached to a conventional electron microscope is suitable for determining the distribution of elements in specimens at a relatively high resolution (1,2). We report here inelastic images of uranyl-stained catalase crystals to 3.4nm resolution. These images were formed by electrons having lost energy with the characteristic energy-loss of uranium (O 4,5) and carbon (K-shell), and show respectively, the stain-occupied (U) and the protein domain (C). Inelastic images were recorded with an electron spectrometer, corrected to second order (3), constructed for a Philips EM (FEG) 400. The energy-loss window (10eV width) was selected at 114eV and 295eV, respectively, for U and C. Pre-edge inelastic images at 100eV (for U) and at 270eV (for C), as well as a dark current image and a gain current image were also recorded for each data set. The dark current image was subtracted from each inelastic image. The difference image was then divided by the difference image between the gain current image and the dark current image. The quotient image was called the normalized image. The normalized "on-edge" image was further divided by the corresponding normalized "pre-edge" image. The quotient image thus obtained eliminates the contrast due to elastic scattering (4), and is a true representation of the distribution of U and C in the catalase crystals. Employing computer image processing techniques of electron crystallography, we extracted phases and amplitudes of Fourier coefficients of these images to synthesize the noise-filtered U and C images. In computer-generated diffraction patterns of these images, the highest reflection order corresponded to a resolution of 3.4nm. The preliminary results of image reconstruction from these data sets indicated that at a resolution of 5.6nm, U and C images were complementary to each other. Supported by NIH Grant HL15835 to the PMI and Training Grant HL07499. REFS: 1) Shuman, H. & Somlyo, A.P., Proc. Natl. Acad. Sci., 79, 106, 1982; 2) Shuman et al., in Scan. Elect. Micros. SEM Inc. II, 737, 1983; 3) Shuman, H., Ultramicroscopy 5, 45, 1980; 4) Johnson, D.E., in Introduction to Anal. Elect. Micros. p. 245, 1979.

**M-AM-B3** QUANTITATIVE MICRO-ELISA FOR RAT INSULIN: CORRELATION WITH RIA, EXTENDED USEFUL RANGE, APPLICABILITY OF CURVE FITTING TO DATA ANALYSIS, AND ASSAY STABILITY. Moore,P.L., Wiechert,S., Didyk,R., MacDonald,M., Bank,H.L. (Intr. by John S. Condeelis) Pathology Dept., Med. U. SC, Charleston, SC 29425.

Recently we developed a micro-Elisa for rat insulin (RI) that is applicable to other insulins. This assay is simple, valid, reproducible, and quantitative. To test how well the results of this ELISA correlate with those of a commercially available RIA, we performed two separate experiments in which the insulin concentrations of 26 experimental samples were measured. Each sample was measured in quadruplicate by each assay. A simple linear regression of the 26 mean insulin concentrations gave an empirical correlation equation of y(ElISA)=0.8x (RIA) 0.5 ng/ml, and a correlation coefficient of r=0.91. The useful range of the ELISA was superior to that of the RIA. For example, the ELISA had a useful range of 0.5-46.0 ng/ml (i.e. 10-920 uU/ml for 90%-10%B/Bo), versus a useful range of 0.2-10.0 ng/ml for the RIA (i.e. 4-200 uU/ml for 90%-10%B/Bo). Since this ELISA is a competitive immunoassay with a sigmoidally shaped standard curve, we sought ways to simplify the dose interpolation and quality control by transforming the standard curve into a straight line relationship with a weighted logit-log transformation (program courtesy of D. Rodbard, NIH). Using data from 4 large precision experiments (12-15 points/curve, n=30/pt), we tested the transformed data for goodness of fit to a straight line (r1=0.99, r2=0.98, r3=0.95, and r4=0.98). Under the same assay conditions, the slope of the standard curves remained the same over a four week period (i.e. ± 2 SEM of average slope, n=4). (NIH# AM 18115-09)

**M-AM-B4** DYNAMIC MICROSCOPE IMAGE PROCESSING SCANNER (DMIPS): A NEW TOOL IN CELL BIOLOGY RESEARCH. Branko Palcic and Bruno Jaggi; Medical Biophysics Unit, B.C. Cancer Foundation, 601 West 10th Avenue, Vancouver, B.C. Canada V5Z 1L3

A new scientific tool, Dynamic Microscope Image Processing Scanner (DMIPS), is being developed for measurements of survival of mammalian cells. After the cells have been treated, they are plated in growth medium in a tissue culture flask where they attach to the bottom surface. DMIPS was originally designed to quickly and automatically recognize a large number of live unstained cells in such a flask. Subsequent measurements of cell growth of previously identified cells can also be done automatically. Thus cell division and/or other cell growth characteristics can be measured in a very large sample yielding precise and statistically significant data. This method is particularly useful in cell survival measurements in the very low dose region where either no experimental data exists, or if they do, they are limited to small numbers of imprecise measurements and are thus associated with large experimental and statistical uncertainties.

During the development of DMIPS, it became apparent that this device could be modified, with sufficient research and development effort to produce a general scientific tool for use in cell biology and medicine. There are many applications, in particular in diagnostic and prognostic medicine where a very large number of cells must be examined in detail as generally few of the cells have special morphological or other properties.

**M-AM-B5** Reverse Immunoaffinity Chromatography of Human Erythropoietin. Paul L. Huang, Philip L. Huang and Sylvia Lee-Huang, Dept. of Biochemistry, New York University School of Medicine New York, New York, 10016.

We report the design and development of a novel immunoaffinity technique of general application that is based on a new principle: reverse immunoaffinity chromatography (RIAC). Antibodies against impurities commonly present in crude preparation of human erythropoietin (Ep) were produced, covalently linked to a solid support and used in whole as an immunoadsorbent. When partially purified Ep was processed by such a column, its contaminating impurities were bound to their antibodies, retained on the column and thus eliminated. In this way, pure Ep can be recovered from the effluent. This method has several advantages, most importantly, it immunoadsorbs the contaminating impurities so that homogeneous antigen and antibody are not required for the preparation of pure Ep. This procedure is particularly useful when the antigen is a weak immunogen such as Ep and its contaminants are difficult to remove by conventional methods. The purified Ep is homogeneous by several criteria. From SDS-PAGE runs a single band with a molecular weight of 34K daltons was obtained. From gel isoelectric focusing a single component with a pI of 4.1 was calculated. Gel electrophoresis in a non-dissociating system at pH 9.6 also resulted in a single band. This material has an average specific activity of 66,000 units/mg of protein as measured by the exhypoxic polycythemic mouse bioassay. The principle of this prototype RIAC methodology should be useful for the purification of other proteins. Supported by NIH grant HL21683.

**M-AM-B6** DIFFERENTIAL MICROSCOPY Wm. Mickols, *M.F. Maestre, I. Tinoco, Jr., Dept. of Chem., Univ. of Cal., Berkeley, Ca., and *Lawrence Berkeley Lab., Berkeley, Ca.

We have built a microscope that forms an image based on the difference in image intensity for two different forms of polarized light. The polarization of the light is controlled by the voltage applied to an electro-optic modulator. We have used linear dichroism to image the aligned hemoglobin polymer within deoxygenated erythrocytes containing mutant sickle hemoglobin (HbS). Taking two linearly dichroic images which are rotated by 45 degrees (or rotating the polarization by 45 degrees) allows the separation of orientation from concentration. We can then present three images, one being dependent on total hemoglobin, the second being concentration of the completely aligned polymer, and the third image being the orientation of the aligned polymer within the cell. It is hoped that this quantification of the amount of aligned hemoglobin polymer within erythrocytes will allow an understanding of the kinetics and mechanism of the alignment of HbS polymer. Imaging on and off the Soret band of the hemoglobin allows us to estimate the small reflection polarization contribution in our measurements of aligned polymer. Reflection polarization is due to the difference in index of refraction inside and outside the cell and to the surface of the cell not being perpendicular to the light vector.

Differential images of biological cells based on circular dichroism can provide information about chiral molecules within them. Intrinsic or induced circular dichroism may allow us to determine spatial changes in the amount and type of nucleic acid within cells.

**M-AM-B7** FLUORESCENCE PHOTOACTIVATION AND DISSIPATION (FPD). Laura J. Brvenik, Ruth Furukawa, Grant A. Krafft, and Bennie R. Ware, Department of Chemistry, Syracuse University, Syracuse, New York 13210 (Intr. by Lindsay Plank)

Fluorescence photobleaching recovery (FPR) has become a popular technique for the study of translational motion in biological membranes, solutions, and complex media. FPR distinguishes among equivalent labeled species by photobleaching a portion of those species in a defined spatial region of the specimen. The redistribution of labeled and unlabeled species is detected by measuring the recovery of fluorescence in the region where photobleaching occurred, and the time scale of this redistribution characterizes the mobility of the labeled species. We have developed the positive analog of FPR, which we call fluorescence photoactivation and dissipation (FPD). FPD involves labelling the species of interest with a new class of molecules, photoactivable fluorophores (PAF's), that are not fluorescent until photochemically converted to fluorophores by an intense pulse of light. This new methodology has three primary advantages over FPR. (1) FPD has an intrinsically higher sensitivity since it involves a high-contrast measurement of a bright signal against a dark background. (2) FPD permits the fluorescence-assisted monitoring of the long-term distribution of species activated in a specific region of the sample. (3)FPD utilizes photochemical reactions that can be designed to be highly specific and much milder than typical photobleaching reactions. We demonstrate in this presentation the types of signal levels achievable with FPD and the design and implementation of a number of PAF's. We will also discuss areas in which this new methodology can be expected to have the greatest impact. (Supported by NIH Grant No. GM-33864 and NSF Grant No. PCM-8306006)

**M-AM-B8 CHLOROTETRACYCLINE FLUORESCENCE IS A SENSITIVE MONITOR OF $CA^{2+}$ HANDLING BY THE HUMAN PLATELET AND IS A USEFUL DIAGNOSTIC OF PLATELET ABNORMALITIES IN VASCULAR OCCLUSIVE DISEASES.** **Wenche Jy, Yeon S. Ahn, William J. Harrington and Duncan H. Haynes, Dept. of Pharmacology, Center for Blood Diseases, University of Miami School of Medicine, Miami, FL 33101.**

**The chlorotetracycline (CTC) fluorescence signal is shown to be a linear measure of the level of free calcium in the dense tubules and in the mitochondria of the human platelet. This is demonstrated in experiments in which the calcium concentration in the cytoplasmic compartment is directly manipulated by the calcium ionophore A23187 and is measured in parallel experiments with Quin 2, a high-affinity cytoplasmic $Ca^{2+}$ indicator. Our studies show that hyperactive platelets are readily and reliably diagnosed by the CTC technique. Addition of 2 mM $Ca^{2+}$ to platelets isolated from patients results in higher levels of dense tubular and mitochondrial accumulation than normal controls. The following ratios of abnormal/normal accumulation were observed in patients with the following diseases - venous thrombosis: 2.01, n = 20; arterial thrombosis: 2.23, n = 17; ITP: 1.74, n = 26; vasculitis: 1.85, n = 13; myelofibrosis: 1.8, n = 21. These findings indicated that activation of plasma membrane $Ca^{2+}$ channels was responsible for the abnormal $Ca^{2+}$ handling. This led us to medicate patients with nifedipine. Normalization of $Ca^{2+}$ handling was observed in platelets of 19 of the 23 medicated patients and clinical improvement was generally observed. Our results are an example of how a "biophysical" probe can be a clinical diagnostic and a monitor of drug efficacy. Supported by USPHS GM 23990.**

**M-AM-B9** A NEW NIH BIOTECHNOLOGY RESOURCE: THE NSLS X-RAY MICROPROBE FACILITY.* A. L. Hanson, B. M. Gordon, and K. W. Jones, Brookhaven National Laboratory, Upton, NY 11973 (Introduced by Stephen W. Feldberg)

The National Synchrotron Light Source (NSLS) X-Ray Microprobe Facility is to be used in part as a new NIH Biotechnology Resource for sensitive trace element measurements. The facility is to utilize the NSLS as a very high brightness source of x rays in the energy range from 3-20 keV. Focussing and collimation of the x rays will be used to produce intense beams with sizes down to the range of 5-10 μm. The x-ray intensities and energies will be sufficient for trace element determinations from about S to U with sensitivities around 100 ppb for small samples and around 10 ppb for bulk measurements. Measurements may be made in vacuum or nonvacuum conditions with wet or dry samples. Design parameters and considerations for the microprobe will be given and the results of preliminary experiments by different groups at several synchrotron storage rings will be summarized. The mode of operation of the Resource will be outlined and procedures for its use explained.

*Supported by NIH under Grant No. 1 P41 RR01838-01 and the Processes and Techniques Branch, Division of Chemical Sciences, Office of Basic Energy Sciences, US Department of Energy, Contract No. DE-AC02-76CH00016.

**M-AM-B10** AUTOMATIC GENETIC ANALYSIS MACHINE (AGA)

R.S. Ledley, D. Gersten, E.J. Zapolski, T.J. Golab, L.S. Rotolo

We have developed an instrument called the AGA (Automatic Genetic Analysis) machine which automates the Southern type nucleic acid hybridization (without blotting). The operator starts with a gel on which the DNA has been placed. The machine automatically carries out electrophoresis, drying, hybridization, stringent washing, and detection operations. The machine is preloaded with radioactive probes for the sequences being investigated and the resulting printout and graphical display contains the same information as that obtained by the manual Southern Blot method, namely a series of bars giving the various intensities for each lane. The entire procedure is automatic and the time it takes depends on the particular experiment being accomplished. However, the time can conservatively be estimated as being less than one-fifth to one-tenth the time it would take to perform the procedure manually. At the moment, eight different probes can be hybridized simultaneously, but expansions are planned. In addition, it is planned to further reduce the time substantially.

**M-AM-B11** METACHROME INSTRUMENT

L.S. Rotolo, R.S. Ledley, T. Golab, J.B. Wilson, M.R. Shiu

The purpose of the Metachrome Instrument is to assist the cytogeneticist in performing certain procedures associated with the analysis of a patient's chromosomes. The Instrument assists the technician in performing two of the most time-consuming procedures, namely that of locating good chromosome spreads on the glass microscope slide and that of constructing the karyotype and recording the alignment classification image. The Metachrome Instrument assists in performing these procedures through the use of computerized automation coupled with electronic and photographic displays. The use of the computer system is highly interactive, and the cytogeneticist makes all final decisions, selections, and reviews. The system is "menu driven" and has been especially designed to be "user friendly".

The automatic computerized metaphase finding operation results in the logging of the coordinates of each metaphase spread found, as well as the preliminary computerized ranking of each such spread. This process is carried out at high speed, where the total length of time required depends on user-selected endpoint criteria, such as the area of the slide to be covered, or number of spreads to be found of a given rank, etc. The chromosome spreads thus found are then shown to the cytogeneticist by the Metachrome Instrument in ranked order for selection for karyotyping.

The karyotyping process can be either carried out automatically by the computer, or the system will also enable karyotyping by the cytogeneticist if desired. The end result of karyotyping is the electronic display of the karyotype, which can then be edited and interactively adjusted to the satisfaction of the cytogeneticist.

**M-AM-B12** AN ENZYME ELECTRODE FOR THE QUANTIFICATION OF ORGANIC PHOSPHONOFLUORIDATES:

K. S. Rajan and S. Mainer, IIT Research Institute, Chicago, IL 60616,
F. C. G. Hoskin, Illinois Institute of Technology, Chicago, IL 60616 and L. Luskus
Brooks AFB, Texas

An enzyme electrode consisting of DFPase attached to the sensing tip of a $F^-$ ion electrode has been prepared for the determination of the toxic organophosphates, i.e., diisopropylphosphorofluoridate (DFP) and pinacolymethylphosphonofluoridate (SOMAN) in aqueous solutions. The electrode-bound enzyme hydrolyzes DFP (and SOMAN) to produce a fluoride ion which is then sensed by the electrode. The enzyme, DFPase, was prepared from squid head ganglia and purified according to the method of Hoskin and Long. Two different electrode combinations were used in this study. By using the DFPase electrode in conjunction with a Ag/AgCl reference electrode the total concentration of unhydrolyzed DFP (and SOMAN) and free $F^-$ produced by non-enzymatic DFP (and SOMAN) hydrolysis was measured. By using the enzyme electrode in conjunction with a combination fluoride ion electrode as the reference, the "unhydrolyzed DFP (and SOMAN)" concentration was measured. The electrode responses ranged from 32 mv to 159 mv for the first system and from -100.6 mv to -22.3 mv for the second. The electrode responses were linear over the range of DFP (and SOMAN) concentration, i.e., $1 \times 10^{-3}$M - $1 \times 10^{-6}$M. The theoretical basis of the DFPase electrode and its application to other cholinesterase inhibitors will be discussed.

M-AM-C1 AMILORIDE BLOCKABLE ION TRANSPORT IN CANINE LINGUAL EPITHELIUM. Sheella Mierson, John A. DeSimone, Gerard L. Heck, and Shirley K. DeSimone, Physiology and Biophysics, Medical College of Virginia, Richmond, VA 23298.

We have established that amiloride blockable ion transport in the lingual epithelium plays a role in salt taste transduction. When the canine dorsal lingual epithelium is placed in an Ussing chamber, the transepithelial potential difference (PD) is 18.1 ± 0.7 mV, short-circuit current (Isc) is 36.1 ± 1.9 $\mu A/cm^2$, and tissue resistance (R) is 517 + 29 $\Omega$-$cm^2$ (mean ± SEM, n=20). The tissue responds to hyperosmotic NaCl (up to 1M) in the mucosal bath with increased PD and Isc and decreased R. This increase in Isc is blocked by ouabain and is partially inhibited by amiloride. Amiloride ($10^{-4}$ M) selectively inhibits the response to luminal hyperosmotic NaCl with little or no effect on the response to KCl in four distinct systems: an in vitro preparation of dog or rat lingual epithelium, neural recordings from the rat chorda tympani in vivo (Heck, Mierson, & DeSimone, 1984, Science, 223:403), single unit recordings in the rat nucleus tractus solitarius and psychophysical experiments in humans (Schiffman, Lockhead, & Maes, 1983, PNAS, 80:6136). Voltage-clamp studies in symmetrical Krebs-Henseleit buffer show that the canine lingual epithelium actively absorbs $Na^+$ and to a lesser extent actively secretes $Cl^-$. $Na^+$ absorption accounts for 46% of the Isc; flux studies demonstrate that there are two transcellular $Na^+$ pathways, one amiloride-sensitive and one amiloride-insensitive. Dose-response curves in vitro for amiloride and several amiloride analogs, using 0.3 M NaCl as the stimulus and Isc as the measure of the response, indicate two amiloride-sensitive transport processes. The results show that at least one type of mammalian salt taste receptor is an apical transport pathway.

M-AM-C2 CHARACTERIZATION OF MEMBRANE PROTEIN COMPONENTS OF LLC-$PK_1$ EPITHELIA BY EPR SPIN-LABEL TECHNIQUE. A.E. Lunsford, A. Moran and C.E. Swenberg, (Sponsor: D.R. Livengood) Biological Spectroscopy Division, Armed Forces Radiobiology Research Institute, Bethesda, MD 20814

Cultured porcine kidney cells (LLC-$PK_1$) exhibit Na-coupled glucose transporter molecules localized at the apical membrane. It has recently been demonstrated that epithelia grown in medium containing 5mM glucose have significantly increased hexose transport capacity and greater numbers of carrier molecules as compared with epithelia grown in 25mM glucose. However, the increase in transporters did not fully account for the enhanced transport capacity. In this study cells grown in medium containing 5mM glucose (5mM cells) and in medium containing 25mM glucose (25mM cells) were spin-labelled, under identical conditions, with 4-maleimido-2,2,6,6-tetramethylpiperidinooxyl, a nitroxide derivative which covalently binds sulfhydryl groups. EPR spectra of the labeled cells clearly exhibited the weakly (w) and strongly (s) immobilized components characteristically observed with use of this spin label on membrane proteins. Analyses of the data resulted in the following observations: (1) The number of sulfhydryl groups labeled per cell was much greater in the 5mM cells; $N_{SH}(5mM) / N_{SH}(25mM) = 2.5$. This corroborates earlier findings that more (protein) transporters are present. (2) When the w/s ratios (the "disproportionation" constants) of the two groups were compared it was found that the 5mM cells have a much greater percentage of weakly immobilized components; $w/s_{(5mM)} / w/s_{(25mM)} \approx 2$. In that former studies have shown that the w fraction corresponds to an "exposed" population, residing nearer the aqueous interface of the membrane, one can conclude from these findings that a larger percentage of the membrane proteins present in the 5mM cells are exposed to the surface environment than those of the 25mM cells. The conclusion is significant in that the 5mM cells have been found to be much more affected by ionizing radiation; the greater percentage of exposed proteins is consistent with susceptibility to attack by radicals at the membrane surface.

M-AM-C3 OSMOTIC WATER PERMEABILITY OF APICAL AND BASOLATERAL CELL MEMBRANES OF PROXIMAL STRAIGHT KIDNEY TUBULE (PST). Paola Carpi-Medina, E. Gonzalez, H. Linares and G. Whittembury. Instituto Venezolano de Investigaciones Científicas, IVIC, P.O. Box 1827, Caracas 1010A, Venezuela, and Escuela de Medicina J.M. Vargas, UVC, Caracas, Venezuela.

Evaluation of osmosis as the mechanism responsible for water absorption in leaky epithelia requires knowledge of the osmotic water permeability of the whole epithelium ($P^e_{os}$), of apical ($P^a_{os}$), basolateral ($P^b_{os}$) cell membranes and of ($P^p_{os}$) that of the paracellular pathway, to construct the adequate hydraulic equivalent model and to test its validity. $P^a_{os}$ and $P^b_{os}$ are in series as water would cross both cell membranes in sequence. Therefore the cell osmotic permeability $P^c_{os} = P^a_{os}.P^b_{os}/(P^a_{os}+P^b_{os})$ and $P^e_{os} = P^c_{os} + P^p_{os}$. Isolated rabbit PST were mounted between holding pipettes. Osmotic steps, $\Delta C$, were produced across the apical cell membrane, to measure $P^a_{os}$, by perfusing the lumen with double barreled micropipettes at 0.5-0.8 nl/s. $\Delta C$ = 15-46 mOsmolar were induced with mannitol. Iso- and anisoosmotic fluids were alternated through the pipette barrels. Changes in lumen diameter were recorded as a function of time with a TV camera and an integrator-processor system (Pflügers Arch.400:343,1984) which provides on-line recordings with space and time precision of 0.03µm and 16.7 ms. The tubules were bathed with oil to diminish basolateral equilibration. Outer tubule diameter was time invariant. $P^a_{os}$ was thus calculated from cell volume changes with time in units of $10^{-4}$ $cm^3/cm^2$ epith.s.Osmolar. The mean was 22.8 ± 1.3 (n=55). With $P^b_{os}$ = 50.4, measured previously, $P^c_{os}$ = 14 (same units). $P^e_{os}$ available values = 40-138. Thus a significant $P^p_{os}$ must exist. $\Delta C$ across the cell membranes of 7-8 mOsmolar is needed if water is to be exclusively absorbed by transcellular osmosis. (Supported in part by CDCH project M-09.5/82. GW is Professor in Instituto Internac.de Estudios Avanzados, IDEA.

**M-AM-C4** SINGLE BASOLATERAL $K^+$ CHANNELS ARE EXPRESSED IN PRIMARY CULTURES OF URINARY BLADDER EPITHELIAL CELLS. John W. Hanrahan, William P. Alles & Simon A. Lewis Dept. of Physiol. Yale Univ. Sch. Med., 333 Cedar St., New Haven, CT 06510

Basolateral potassium conductance is an important feature of the Koefoed-Johnsen & Ussing model for transepithelial $Na^+$ absorption. We recently described a 200 pS $K^+$ channel in the basolateral membrane of freshly dissociated rabbit urinary bladder epithelial cells (J. Gen. Physiol. 84:30a,1984). In an effort to increase our rate of obtaining gigaohm seals, we extended this study to cells grown in primary culture, and have found this channel in the surface membrane of sub-confluent cultures. In excised patches, the mean single channel conductance was 217 pS in 150 mM KCl solution. Power density spectra of the currents recorded at ~22°C could be fitted with two Lorentzian-type components having corner frequencies of approximately 11 and 250 Hz, similar to those obtained in dissociated bladder cells (9 and 272 Hz, respectively). Channels from both sources were unaffected by $Ca_i^{2+}$ and blocked by barium; and for both channels, the open-state probability increased with membrane depolarization. In dissociated cells, this dependence approached a slope of e-fold/9 mV. Transitions sometimes occurred in groups, with active and quiescent periods each lasting 5-10 seconds. At hyperpolarized potentials, the durations of open ($\bar{t}_o \simeq 21$ ms) and closed events ($\bar{t}_c \simeq 61$ ms) accounted for the low-frequency component of the power spectrum. Bursts were prevalent at depolarized potentials. Finally, there is a state having 65% of the full open-channel conductance, but it was rarely observed. Sub-confluent primary cultures of epithelial cells may provide a convenient model for studying the properties and modulation of basolateral ion channels. Supported by NSERC & MRC(Canada) fellowships and NIH 33243.

**M-AM-C5** VOLTAGE-DEPENDENT CHLORIDE CONDUCTANCE OF TOAD SKIN: LOCALIZATION BY VIBRATING PROBE. Carl Scheffey and Uri Katz. Marine Biological Laboratory, Woods Hole, and Technion, Haifa, Israel.

The skin of the toad Bufo viridis has a voltage-dependent chloride conductance which activates over tens of seconds when the skin is polarized outside negative (Katz and Larsen, J.Exp.Biol. 109:353). We used the vibrating probe technique in combination with Ussing chamber (as in J.Membr.Biol. 75:193) to localize this chloride pathway on the surface of the epithelium. Epithelia from toads salt adapted for several days (Katz and Larsen, ibid.) were clamped to -100 mV (outside negative) and scanned with the vibrating probe. Peaks of current density were observed over a portion of the mitochondria-rich cells and nowhere else. Peaks had highly variable sizes. After a step to -100 mV from short circuit, the probe-measured peak of current at a mitochondria-rich cell activates with the same time course as the known voltage-dependent chloride current. It appears that the voltage-dependent chloride conductance is localized to a subpopulation of the mitochondria-rich cells.

Supported by NIH RR01395-03.

**M-AM-C6** SUBSTANCE P AND RELATED TACHYKININS ON ISOLATED CANINE TRACHEAL EPITHELIUM, P.K. Rangachari, D.McWade* (Dept. of Medicine and Intestinal Disease Research Unit) McMaster University, Hamilton, Ontario, Canada, L8N 3Z5. The response of the isolated canine tracheal epithelium to Substance P (SP) is dependent on the side to which the peptide is added. Serosal addition ($10^{-7}$ M) produces an increase in P.D. and a decrease in resistance, following a lag of 55.8 sec (range 40-90 sec) with the maximal value being obtained after 2.5 min (range 1.5-4 min). Luminal addition ($10^{-7}$ M) produces an initial decrease in P.D. ("dip") within 11 sec (range 8-20 sec) followed by an increase in P.D. beginning by 21.5 sec (range 12-40 sec) reaching a peak value after 56.5 sec (range 40-90 sec). On serosal addition the dip was never noticed. Replacement of chloride by isethionate aborted the dip whereas substitution with nitrate considerably exaggerated the response. With low doses ($5 \times 10^{-12}$ M) only the increase in P.D. was noted with the dip appearing at concentrations that were 10-100 fold higher. It appears that the peptide produces 2 distinct responses, perhaps on two different cells but certainly on receptors with two different affinities. The initial decrease in P.D. appears to require a permeant anion. Related peptides were studied. Luminal addition of physalaemin, kassinin, eledoisin, $\alpha$-neurokinin, neuromedin K and C-terminal SP fragments larger than 5 amino acids gave positive responses. No responses were noted with litorin, bombesin, neurotensin, dynorphin or SP 8-11 and SP 1-9. The peptide sequence Phe-X-Gly-Leu-Met $NH_2$ seems necessary to elicit the luminal response.

Supported by Canadian Cystic Fibrosis Foundation.

**M-AM-C7** CALCIUM-INDUCED POTASSIUM EFFLUX IN SUSPENSIONS OF MAMMALIAN RENAL PROXIMAL TUBULES. S.R. Gullans, G. Capasso*, M.J. Avison*, and G. Giebisch. Department of Physiology, Yale Univ. School of Medicine, New Haven, CT 06510

Previous studies by numerous investigators have shown that increases in cytosolic calcium can alter sodium transport and/or the membrane permeability to potassium. We have explored this phenomenon in the renal proximal tubule. Suspensions of rat and rabbit renal cortical tubules were prepared by collagenase infusion of the kidneys. This preparation is enriched in proximal tubules (> 90%) which have open lumens. Tubules (6-10 mg protein/ml) were suspended in a standard bicarbonate Ringer (5% $CO_2$, pH 7.4) and placed in a chamber (37°C) containing a $K^+$ electrode to monitor extracellular $K^+$ concentration. Inhibition of $Na^+,K^+$-ATPase activity by either anoxia or ouabain ($10^{-4}$ M, rabbit only) caused an immediate and rapid release of $K^+$ by the tubules. This efflux was severely blunted by $Ba^{2+}$ (1 mM), a known inhibitor of $K^+$ channels. Conversely, addition of $Ba^{2+}$ (1-5 mM) to the tubules caused a rapid uptake of $K^+$. TEA (1 mM) had no effect. In another series of experiments, A23187 ($10^{-6}$ M), which can increase cytosolic $Ca^{2+}$, caused a slow (20 min.) release of cellular $K^+$. Similarly, ruthenium red (3 x $10^{-6}$ M), which can elevate cytosolic $Ca^{2+}$ by blocking mitochondrial $Ca^{2+}$ uptake, caused a slow release of cellular $K^+$ although an initial 1 minute lag period was observed. We conclude that an extracellular $K^+$ electrode can monitor net fluxes of $K^+$ related to changes in $Na^+,K^+$-ATPase activity and $K^+$ permeability. Furthermore, increases in cytosolic $Ca^{2+}$ cause a net efflux of $K^+$ presumably by inhibiting $Na^+,K^+$-ATPase activity or by activating a $Ca^{2+}$-sensitive $K^+$ channel.

**M-AM-C8** BINDING OF AMILORIDE BY DNA. C. J. Costa, L. B. Kirschner and E. J. Cragoe, Jr. Dept. of Zoology, Washington State University, Pullman, WA 99164-4220 and Merck, Sharp and Dohme Research Laboratories, West Point, PA 19486. EPR spectroscopy showed that a 10K x g centrifugal fraction from homogenates of Na transporting epithelia (fish gill and kidney) has a reversible amiloride (Am)- binding membrane (Costa et al, Biophys. J. 41; 195a; 1983). This was absent from muscle and liver fractions and was identified as apical membrane from Na transporting epithelial cells. We report here that DNA found in the 10K centrifugal fraction, also shows reversible binding of the spin-labelled amiloride derivative (ASp). With 3 x $10^{-6}$M ASp, binding increased linearly with [DNA] over the range 0-50 µgm/ml and was completely displaced by an excess of unlabelled Am. At higher [DNA] total binding increased but was only partly displaceable. In the lower range about 10 nmole ASp was bound/mg DNA. The 10K centrifugal fraction from kidney contained 18 µgm DNA/mg protein so a fraction of the binding might be due to DNA rather than to membrane Am-binding sites. However, the value found for pure DNA suggests that ASp binding to DNA in the 10K fraction amounts only to about .01 nmole/mg protein. Total displaceable binding by this fraction is 3-15 nmole/mg protein. Treatment of the 10K fraction with DNAase reduced DNA to 4 µgm/mg protein, but had only a minor effect on ASp binding. Both observations support the original conclusion that ASp is bound to a membrane in the 10K fraction, not to DNA. A number of recent reports show that amiloride interferes with the synthesis or expression of DNA in cells. Our results suggest that Am may act directly on the nuclear DNA rather than through an effect on $Na^+$ transport. Supported by NSF 8309153.

**M-AM-C9** EFFECT OF TEMPERATURE ON THE TRANSMEMBRANE POTENTIAL OF LIVER CELLS. Robert Wondergem and LaVerne R. Benner. Physiology Department, Quillen-Dishner College of Medicine, East Tennessee State University, Johnson City, TN. 37614. (Intr. by W. McD. Armstrong).

We have measured effects of altering temperature on the steady-state transmembrane potentials ($E_m$) of liver cells. The purpose was to determine if liver $E_m$ varied as a function of temperature as predicted by diffusion kinetics. $E_m$ of hepatocytes in mouse liver slices were measured using conventional glass microelectrodes filled with 0.5 M KCl and having tip-resistances of 10-20 M ohms. Effects of changes in temperature from control (37°C) on liver $E_m$ were determined during continuous recordings of $E_m$ in single cells. $E_m$ varied as a linear function of temperature. The temperature coefficient ($Q_{10}$) of 1.61 was greater than 1.033 predicted for a direct proportional of absolute temperature. This difference was unexpected since the resting $E_m$ of excitable cells is propotionate to absolute temperature and in accord with the temperature parameter of the Goldman equation. $Ba^{++}$ and quinine, which block $Ca^{++}$-activated $K^+$ channels, reversibly inhibited temperature-dependent increases in hepatocyte $E_m$. We conclude that effects of temperature on liver $E_m$ do not result from temperature effects on membrane $K^+$ channel conductance alone. The results also are consistent with a temperature effect on kinetic parameters for opening and closing of membrane $K^+$ channels by altering either intracellular $Ca^{++}$ activity or $Ca^{++}$ binding to channel proteins. Supported by the Kroc Foundation.

**M-AM-C10** FLUORESCENT LABELING OF THE LUMINAL MEMBRANE OF THE TRACHEAL EPITHELIUM. Carole M. Liedtke. From the Cystic Fibrosis Center, Departments of Pediatrics and Developmental Genetics and Anatomy, Case Western Reserve University, Cleveland, OH 44106.

The luminal surface of the tracheal epithelium was labeled with a complex of fluorescamine with cycloheptaamylose (CFC) prepared according to the method of Nakaya, et.al. (Biochem. Biophys. Res. Comm. 67:760-766, 1975). A solution of CFC was prepared to a final concentration of 2 mg/ml in Hank's balanced salt solution, pH 8.3 (HB8.3). Rabbits were killed by intravenous injection of pentobarbital and the trachea immediately excised and transferred to Hank's balanced salt solution, pH 7.4 (HB7.4). Extracartilagenous tissue was dissected from the trachea which was then opened along the posterior border and pinned open on a dissection board with the luminal surface up. The surface of the trachea was washed with HB8.3 then flooded with the CFC solution. The tissue was incubated for 20 min. at room temp. under a high intensity lamp, rinsed free of unreacted CFC and flooded with HB7.4 lacking $Ca^{+2}$ and $Mg^{+2}$ but containing 135 Units collagenase/ml, 15 mM EDTA and 1 mM dithiothreitol. After 45 min. incubation at room temp. under a high intensity lamp, the surface epithelium was hand dissected from the underlying submucosal tissue and transferred to HB7.4. In unstained preparations, cilia on ciliated cells continued to beat. Under phase microscopy, intact single cells and sheets of surface epithelium were easily identified. Fluorescence was detected only on the luminal surface of the epithelium and cells. In particular, cilia displayed intense fluorescence indicating labeling of the ciliary membrane. The results indicate that CFC may be a nonpenetrating probe of the luminal plasma membrane of tracheal epithelial cells. The research was supported by grants from the NIH (NIRA, HL 27700) and the Cystic Fibrosis Foundation, Rainbow Chapter.

**M-AM-C11** A PATCH-ELECTRODE STUDY OF MEMBRANE POTENTIAL, RESISTANCE, AND CHANNEL SWITCHING IN ISOLATED MOUSE FIBROBLASTS. Shigeru Hosoi and Clifford L. Slayman, Department of Physiology, Yale University School of Medicine, New Haven, CT 06510.

The whole-cell patch-electrode technique has been applied to single suspension-cultured mouse fibroblasts. Rupture of the membrane patch inside the electrode was accompanied by a shift of measured potential into the range -10 to -25 mV, but with little change in the recorded resistance. Steady-state current voltage curves were generated before and after rupture of the membrane patch, and the difference between these gave zero-current membrane potentials of -50 to -75 mV, which represents a leak-corrected estimate of the true cell membrane potential. The associated slope conductivity of the cell membranes was 5-15 $uS/cm^2$ (assumed smooth-sphere geometry, cells 13-15 um in diameter) and was potassium-dominated. With 0.1 mM (or more) free calcium filling the patch electrode, membrane potentials in the range -60 to -85 mV were observed following patch rupture, with associated slope conductivities of 200-400 $uS/cm^2$, also potassium dominated. Similar voltages and conductivities were observed at the peak of pulse-induced "hyperpolarizing activation" (Nelson, Peacock, & Minna, J. Gen. Physiol. 60:58-71, 1972), and the two phenomena probably reflect the behavior of $Ca^{++}$-activated $K^+$ channels. Single channel recordings in cell-attached and excised-patch modes showed two classes of channels. Small inward-rectifying channels have conductances near 20 pS, and conspicuous large channels have conductances up to 300 pS. The two classes probably correspond, respectively, to the normal $K^+$ conductance and the $Ca^{++}$-activated $K^+$ conductance observed in the whole-cell recordings.

Supported by Research Grants PCM-7913412 from N.S.F., and AM-17433 from N.I.H.

**M-AM-D1** NUCLEIC ACID JUNCTIONS ARE NOT HIGHLY FLEXIBLE. +Rong-Ine Ma, +Neville R. Kallenbach and *Nadrian C. Seeman, +Dept. of Biology, Univ. of Pennsylvania, Philadelphia, PA 19104 and *Dept. of Biological Sciences, SUNY Albany, Albany, NY 12222.

We have recently shown that the minimization of sequence symmetry can yield stable immobile nucleic acid junctions, formed from oligonucleotides.[1] Nucleic acid junctions constitute valence clusters, which, in principle, can be connected to form stick figures in space. In each of these possible polygons, polyhedra or N-connected networks, the junction constitutes a vertex, while the edges are double helical nucleic acid. We have shown that enzymatic oligomerization of a 3-arm sticky-ended junction produces covalently closed 4- and 6-component space curves, with about 2 turns of DNA between vertices; 3-, 5- and 7-component closed products are conspicuously absent. This finding has been determined from the appearance of only these species of closed single-stranded molecules on denaturing gels. In a companion experiment, 4-arm junctions have been oligomerized in a blunt-ended ligation reaction, resulting in about 1.5 turns of DNA between junctions. In this non-integral system, small, closed, single-stranded circles should only result from bending or twisting of the junction components, since linear DNA of the short lengths involved is unlikely to close on itself. Although a ladder of products through decamers has been seen, no closed single-stranded circles have been obtained. These results suggest that the flexibilities of 3-arm and 4-arm nucleic acid junctions are not grossly different from that of linear DNA.

[1]N.R. Kallenbach, R.-I. Ma and N.C. Seeman, Nature 305, 829-831 (1983).

This work has been supported by grants ES-00117, GM-29554 and CA-24101 from the NIH.

**M-AM-D2** RAMAN SPECTROSCOPIC STUDIES OF THE TEMPERATURE-INDUCED B→ Z TRANSITION IN POLY [d(G-$m^5$C)] Daniel M. Brown and Roger M. Wartell, School of Physics, Georgia Institute of Technology, Atlanta, Georgia 30332.

Laser Raman spectra of the synthetic polynucleotide poly[d(G-$m^5$C)] (60 mg/ml) in 50 mM NaCl, 20 mM $MgCl_2$ have been obtained at temperatures ranging from 5°C to 45°C. Under these conditions, the polymer undergoes a cooperative transition from the right-handed B conformation (T<20°C) to the left-handed Z conformation (T> 40° C). Changes in the intensities of Raman peaks at 576, 622, 681, 752, 782, 835, 1265, 1312, 1331, 1354, and 1363 $cm^{-1}$ were observed in spectra taken at 5° C intervals during the course of the B→ Z transition. Raman peaks were quantified with a computer analysis procedure using a polynomial function to approximate the background, and Lorentzian functions convoluted with the instrument function to represent the bands. Peak heights were compared between different experiments by normalizing to the 1176 $cm^{-1}$ peak height; the peak height of this band did not appear to change in these experiments. The deconvolution showed that the 782, 835, 1265, 1312, 1354, and 1484 $cm^{-1}$ peaks are better fit by composites of several Raman bands, which change in both intensity and frequency during the B→ Z transition. Plots of the relative peak heights as a function of temperature show bi-phasic transition curves; the curves are characterized by an abrupt transition between 20° - 30°C with more gradual intensity changes between 30° - 40°C. The shapes of the transition curves were similar for most of the peaks measured, including both base-specific and DNA backbone-specific vibrational modes; accordingly, changes in the base and backbone conformations have the same temperature-dependence in the transition. These results are compared to a Raman study of the B - Z transition in poly[d(G-C)] where the transition is induced by increasing the solvent ionic strength. Supported by N.I.H.

**M-AM-D3** THE TETRANUCLEOTIDE rCGCG CAN ADOPT A LEFT-HANDED Z CONFORMATION. Hall, K.B., Leonhardt, E., Cruz, P., Tinoco, I. Jr., and Neilson, T.*, University of California-Berkeley, Department of Chemistry, Berkeley, CA 94720 and *McMaster University, Department of Biochemistry, Hamilton, Ontario, Canada.

The tetranucleotide rCGCG can adopt either an A or a Z geometry as a function of salt concentration. In 1M $NaClO_4$ at 0°C, it exists in a double-standed A geometry; in 6M $NaClO_4$ at 0°C, in a left-handed, double-stranded Z geometry. Using circular dichroism to determine the conformation of the tetramer in different salt concentrations, we have constructed a phase diagram for A, Z and single strands vs. temperature and salt concentration. There is no A→Z or Z→A transition observed for the tetramer as a function of temperature as there is with poly[r(G-C)] [Nature 311, 584, (1984)]. The $\Delta H$ (A→single strands) and $\Delta H$ (Z→single strands) are compared, and a $\Delta H$ (A→Z) is estimated. $^{31}P$ and $^{1}H$ NMR are being used to help characterize the A and Z geometry. A possible third conformation, induced by 4M $MgCl_2$ will also be described.

**M-AM-D4** THE UNUSUAL PROTON EXCHANGE PROPERTIES OF Z FORM POLY[d(G-C)].

Peter A. Mirau and David R. Kearns. AT&T Bell Laboratories, 600 Mountain Ave., Murray Hill, NJ 07974 and the Department of Chemistry, B-014, University of Cal. San Diego, La Jolla, CA 92093.

Imino proton spin-lattice relaxation rates and real-time solvent exchange have been used to study imino and amino proton exchange in B- and Z-form poly[d(G-C)]. In 4.5 M NaCl the most slowly exchanging protons ( two orders of magnitude slower than in B-DNA) are identified as the guanine imino and the cytosine amino hydrogen bonded to the guanine carbonyl. Both protons exchange at the same rate, follow single exponential exchange kinetics, and cannot be catalysed, implying that the exchange of both protons occurs from the same transient solvent exposed state. The exchange depends strongly on temperature and has the same activation energy (22 kcal/m) as the optically measured B-to-Z transition. In addition, exchange occurs at the same rate as the B-to-Z conversion. The correlation between the B-to-Z kinetics and the proton exchange also extends to 3.25 M $NaClO_4$ solutions, where both rates are a factor of 5 faster. This unexpected parallelism between the B-to-Z transition kinetics and the Z-exchange kinetics indicates that the rate limiting steps in both processes are similar.

**M-AM-D5** IMINO PROTON EXCHANGE RATES OF TWO POTENTIAL Z-DNA FORMING SEQUENCES. M. Donlan, S. Cheung, and P. Lu, Department of Chemistry, University of Pennsylvania, PA 19104.

From our examination of the properties of DNA at regulatory regions, we have observed a higher imino proton exchange rate occurring at the center of a sequence GTG/CAC, in a double helix. Our obersvation was that this particular triplet occurs rather frequently in many prokaryotic and eukaryotic regulatory systems suggesting that it may be part of a general signal for protein interaction.

The eukaryotic transcriptional enhancers of the simian virus 40 contains two GTG/CAC sequences in its critical core region. Nordheim and Rich have suggested that the enhancer may adopt a ZDNA conformation which could be associated with the mechanism of transcriptional enhancement (Nature 303, 674-678, (1983)). The antibodies to Z-DNA used to detect the Zconformation in the SV40 enhancer also protect a sequence in pBR322 from restriction enzyme digestion which contains two GTG/CAC sequences symmetrically arranged. (Nordheim et al, Cell, 31 309-318 (1982).

As a consequence, we have synthesized the SV40 enhancer core consensus sequence and the DNA fragment from pBR322 that is bound by Z-DNA antibodies. The exchange kinetics of the imino proton resonances were examined using saturation recovery methods. The results indicate that there is a higher rate of exchange at the GTG/CAC sequences in both of these DNA fragments analogous to our observations in the lac operator (Proc. Natl. Acad. Sci. USA 81, 3665-69, (1984).

Results from $^{31}$P-NMR studies performed on these sequences will also be presented. (Supported by grants from N.I.H.)

**M-AM-D6** ACTION OF ENHANCER SEQUENCES: IMPLICATIONS OF A NEW GENE CONTROL MECHANISM

R. C. Hopkins, University of Houston - Clear Lake, Houston, Texas 77058

The pairwise interaction of two homologous DNA duplexes to form a tetraplex structure (4-stranded DNA) has been proposed recently as a mechanism of long-term gene regulation and cell differentiation [1]. This scheme is based on an alternative family of double-helical models, Configuration II, which differs in a subtle way from the Watson-Crick family of models, Configuration I, by having antiparallel chains of the opposite sense [2,3]. The implications of the hypothesis are far-reaching indeed: a) it provides a basis for understanding the extreme fidelity of genome maintenance in diploid organisms, b) it offers an explanation of the DNA methylation patterns in higher plants and animals, and c) it suggests a fundamental mechanism in the initiation of carcinogenesis [4]. Furthermore, this gene control model suggests a mode of action for genomic enhancer sequences. It is proposed that these sequences are sites of initial disruption of a tetraplex, where the two transcribable duplexes separate to form a "bubble". As the bubble grows, increasing lengths of duplex DNA are exposed for transcription, which may account for the ability of enhancer sequences to affect gene expression over large genomic distances. For ease of duplex-duplex separation, it is expected that enhancer sequences should be AT rich. (Supported by grant E-889, Robert A. Welch Foundation)

1. Hopkins, R.C. (1984) Comments Mol. & Cell. Biophys. 2, 153.
2. _____, (1981) Science 211, 289.
3. _____, (1983) Cold Spr. Harb. Symp. Quant. Biol. 47, 129.
4. _____, in The Molecular Basis of Cancer: An Interdisciplinary Discussion on Basic and Applied Aspects of Cancer, R. Rein, ed., Alan R. Liss, Inc., N. Y., in press.

**M-AM-D7** EVIDENCE FOR TWO DIFFERENT GLOBAL SECONDARY STRUCTURES OF SUPERCOILED DNAS AND BUFFER-INDUCED SWITCHING. J. Michael Schurr, John H. Shibata, J. Wilcoxon, A. S. Benight, J. Langowski, J. C. Thomas, and B. S. Fujimoto, Department of Chemistry, University of Washington, Seattle, WA 98195.

Different global secondary structures of duplex DNAs can be distinguished by their twisting rigidities, which are manifested in the fluorescence polarization anisotropy (FPA) of intercalated ethidium, and in dynamic light scattering (DLS) at large scattering vector, but not generally by gel electrophoresis (GEL) in tris-borate buffer. In tris buffer supercoiled M13mp7, pBR322, and pUC 8 DNAs exhibit a high value ($\alpha=(4.8\text{-}5.2)\times10^{-12}$ erg) of the apparent torsion constant, whereas in citrate (or cacodylate) buffer M13mp7, pB322 and pHC79 DNAs exhibit a low value ($\alpha=(2.4\text{-}3.0)\times10^{-12}$ erg). DLS at large scattering vector confirms that the rigidities and, hence secondary structures, of supercoiled M13mp7 and pBR322 are different in the two buffers. The transition between secondary structures is extremely slow and rather sharp, which indicates a large junction free-energy. Upon linearization of M13mp7 DNA in tris and cacodylate neither torsion constant immediately assumes the value characteristic of a normal linear DNA, hence neither is a simply strained B-helix. After linearization of M13mp7, pBR322, and pUC 8 in tris the apparent torsion constants evolve for more than 8 weeks before approaching the value for normal B-helix, but GEL mobilities remain normal and constant throughout this evolution period.

Noteworthy observations concerning alternate tertiary conformers of supercoiled M13mp7 and pBR322 have also been made.

**M-AM-D8** EXCITED-STATE PROPERTIES OF NUCLEIC ACIDS AT ROOM TEMPERATURE ON THE PICOSECOND TIME SCALE. S. Georghiou*, Thomas M. Nordlundt, and A. M. Saim*,* Biophysics and Chemical Physics Lab., Dept. of Physics, Univ. of Tennessee, Knoxville, TN 37996-1200 and †Depts. of Radiation Biology-Biophysics and Physics, Univ. of Rochester, Rochester, NY 14642.

We report the first picosecond fluorescence decay time measurements of nucleic acids at room temperature obtained by using 25 ps, 266 nm laser pulses from a frequency-quadrupled Nd:YAG laser and a streak camera-optical multichannel analyzer system that has a time jitter of 2 ps. The systems studied are DNA, DNA with 16% of its G residues methylated at the N-7 position, the corresponding fluorophore 7-methyl GMP, and poly (dG-dC)•poly(dG-dC) (in the B and Z conformations) as well as poly (dA-dT)•poly (dA-dT). The A-T base pairs appear to be the major emitters in DNA. By combining the decay time measurements with measurements of fluorescence quantum yields, we have calculated rate constants of radiative and nonradiative transitions and have obtained evidence for transfer of energy from the other residues to the methylated G residue with an efficiency of ~ 20% and over a distance of ~ 12 base pairs. There are two components in the fluorescence decay profiles of the B and Z conformations of 8 ps and 100 ps and 8 and 150 ps, respectively, with the long-lived component making a smaller contribution in the latter case. This property of the Z conformation as well as its enhanced fluorescence relative to that of the B conformation are potentially useful structural indicators. Supported in part by American Cancer Society grant IN-89H, NSF grants PCM-83-02601 and PCM-80-18488, and by the sponsors of the Laser Fusion Feasibility Project at the Laboratory for Laser Energetics of the University of Rochester.

**M-AM-D9** INFLUENCE OF A CIS-SYN TpT PHOTODIMER ON THYMINE OLIGOMER CONFORMATIONS. R.E. Rycyna and J.L. Alderfer. Biophysics Department, Roswell Park Memorial Institute, Buffalo, NY 14263.

Acetone photosensitized irradiation (200-400kJ/m$^2$ of 310±35nm) of dTpdT, d(TpTpT) and d(TpTpTpT) was found to form predominantly photodimers. Formation of photodimers, represented as T(p)T and abbreviated as D, was monitored using P-31 NMR. Cis-syn photodimers were separated from minor configurational isomers using C18 reverse phase HPLC. Two photodimers are observed in the trimer model (DpT and TpD) whereas four are seen in the tetramer model (DpTpT, TpDpT, TpTpD, and DpD). H-1 NMR spectral characteristics common among these 'positional isomers' and the cis-syn T(p)T reported by Hruska et al., 1975 (Can. J. Chem. 53: 1193) confirm the presence of the cis-syn configuration in these photodimer models. P-31 NMR data of the various oligomers containing these lesions indicates upfield shifts occur for phosphodiesters between the cyclobutyl-linked thymines whereas neighboring phosphates undergo downfield shifts of differing magnitudes relative to the chemical shift positions of unmodified oligomers. Proton-phosphorus coupling patterns and carbon-phosphorus coupling constants of these neighboring or 'perturbed' phosphodiesters indicate the phosphodiester conformation of thymine nucleotides adjacent to cis-syn photodimers are not similar. Significant conformational changes in these adjacent nucleotides are also observed using proton NMR. Cis-syn photodimers are also formed in poly(dT) and conformational perturbation has been investigated using P-31 and H-1 NMR. The data indicates only first nearest neighbor nucleotides in this single strand DNA helix are affected by the lesion. (Supported by N.I.H. 2T32-ES07057 and the GSA at SUNY at Buffalo).

**M-AM-D10** COVALENT BINDING OF (+) AND (-) BENZO[A]PYRENE-ANTI-DIOLEPOXIDE TO B AND Z FORMS OF POLY(dG-dC):POLY(dG-dC) AND POLY(dG-$m^5$dC):POLY(dG-$m^5$dC).
Fu-Ming Chen, Department of Chemistry, Tennessee State University, Nashville, Tennessee 37203

Circular dichroism (CD) as well as absorption spectral measurements reveal that poly(dG-$m^5$dC):poly(dG-$m^5$dC) suffers more extensive covalent modification by (+)-benzo[a]pyrene-anti-diolepoxide (anti-BPDE) than its unmethylated counterpart and the covalently attached pyrenyl moiety exhibits stronger stacking interactions with the bases in the methylated polymer. Modifications due to (+) anti-BPDE on the hexaminecobalt induced Z DNAs are much less pronounced and the pyrenyl spectral characteristics are quite distinct from those of the B-form. Salt titration on the (+) anti-BPDE modified poly(dG-dC):poly(dG-dC) suggests reduced cooperativity on the B to Z transition. Stereoselective binding properties of these polymers are evidenced by the much reduced preference for the (-) enantiomer. The unimpressive covalent binding ability of the (-) isomer can, however, have profound effect on the DNA conformation as evidenced by the near inversion to the B form when the Z form poly(dG-dC):poly(dG-dC) is modified with (-) anti-BPDE. No such effect is observed for the methylated polymer nor the (+) enantiomer.

**M-AM-D11** DYNAMIC-PROGRAMMING ALGORITHMS FOR PREDICTING OPTIMAL AND SUBOPTIMAL SECONDARY STRUCTURES OF RNAs.
Arthur L. Williams, Jr. and Ignacio Tinoco, Jr. Department of Chemistry and Laboratory of Chemical Biodynamics, University of California, Berkeley, CA 94720.

We present three computer methods that predict the secondary structures of an RNA that have the lowest free energies. They are dynamic programming algorithms with different properties that are specially designed to identify alternate equivalent and suboptimal structures, as well as the optimal structure. The most efficient algorithm employs the assumption that RNAs are folded sequentially and that the stability of the previously folded subsequence drives the folding of the next, larger sequence. A second algorithm utilizes a "stem-oriented" approach, so that once an optimum double-helical region or stem has formed the growing stem drives the further folding of the RNA. The most rigorous algorithm is not constrained by such limiting assumptions. It is not exhaustive however. It assumes the pair-wise addition of non-overlapping regions to find optimal closed multi-stem substructures. The range of free energy values above the minimum, for suboptimal structures, determine the time and memory requirements of the three algorithms. The limits set on that range determine whether a dynamic programming procedure can effectively, within practical amounts of time and memory, identify alternate structures. Chemical reactivity, enzyme susceptibility, and phylogenetic data can be incorporated into the algorithms, resulting in biologically more relevant structures. We go beyond other procedures which have appeared in the literature and show how to identify specific secondary structural patterns (such as clover-leafs) among all possible substructures. These methods are illustrated with the foldings of t-RNA, various structural RNA and intron sequences.

**M-AM-D12** DUPLEX: A CRAY-1 ARRAY PROCESSOR PROGRAM THAT MINIMIZES RNA AND DNA CONFORMATIONS.
B.E. Hingerty, Health and Safety Research Division, Oak Ridge National Laboratory, Oak Ridge, Tennessee 37831 and T.L. Hayden, Dept. of Mathematics, Univ. of Kentucky, Lexington, Kentucky 40506.

A new program has been written that minimizes RNA and DNA conformations by employing the Scheraga algorithm and the potentials of Srinivasan and Olson. We are now no longer limited to only two residues, but can extend the calculations to the Dickerson B-DNA dodecamer. Extensive work has been done to optimize the program in order to take advantage of the array processing capabilities of the DOE CRAY-1 computers at Lawrence Livermore Laboratory. The program will also be modified to use the new CRAY-XMP computer, which will be available shortly. Additional work is being done to include the following: hydrogen bond potential, metal ions to neutralize the phosphates, solvent effects, and a new dielectric function employing Debye's theory of ionic saturation. The program will also allow us to study native or unmodified structures as well as those modified by carcinogens or toxic metals. Current progress will be presented at the meeting. This work is done in close collaboration with Professor S. Broyde, Biology Dept., New York University.

Research sponsored jointly by the Office of Health and Environmental Research, U. S. Dept. of Energy, under contract DE-AC05-840R21400 with Martin Marietta Energy Systems, Inc. and PHS Grant 1R01 CA28038-04 awarded by the National Cancer Institute, DHHS, to S. Broyde, Biology Dept., New York University.

M-AM-E1 THEORY OF THE HELIX-COIL TRANSITION IN TWO-CHAIN, COILED COILS. Jeffrey Skolnick, Department of Chemistry, Washington University, St. Louis, MO 63130

A theory of the helix-coil transition in two-chain, coiled coils (dimers) such as the muscle protein tropomyosin has been developed in terms of the intrachain Zimm-Bragg helix initiation, ($\sigma$), and propagation ($s$) parameters and a new interchain helix-helix interaction parameter $w$ that accounts for the enhanced stability of helical states in the two-chain, coiled coil relative to the isolated single chains. The theory includes the effects of loop entropy and the possibility of mismatched association of the two chains. For chains of the length of tropomyosin, loop entropy acts to eliminate interior random coil stretches between interacting helical regions in the dimer. Since loop entropy restricts the number of interacting pairs of helices to one, the only mismatched conformations of the non-crosslinked chains are those that are out-of-register. Loop-entropy by restricting the number of allowed states acts to make the helix-coil transition more cooperative; whereas, the inclusion of out-of-register states makes the helix-coil transition less cooperative.

The theory predicts that the helix-coil transition proceeds by the melting of the helix in the dimer which is in equilibrium with the single chains of much lower helix content. Thus, the observed overall helix-content should be concentration dependent. Since the interhelical interaction is responsible for the greatly augmented helix content of the dimer relative to the single chains, in the limit of high helix, the in-register state should dominate the population. However, as the helix-coil transition proceeds, out-of-register states are predicted to become increasingly important. In the following paper, the theory is applied to the prototypical two-chain, coiled coil, tropomyosin. (Supported by NSF-PCM-83-43209).

M-AM-E2 APPLICATION OF AUGMENTED HELIX-COIL THEORY TO TROPOMYOSIN. Jeffrey Skolnick and Alfred Holtzer, Department of Chemistry, Washington University, St. Louis, MO 63130.

The statistical mechanical theory of the helix-to-random-coil transition in two-chain, $\alpha$-helical coiled coils, has recently been augmented by inclusion of the effects of loop entropy and out-of-register ("mismatched") structures. This theory is applied to experimental data on noncrosslinked $\alpha$-tropomyosin at nearly neutral and at acidic pH. A semi-quantitative fit of the helix content vs. temperature is obtained at each pH, over a thousand-fold range of protein concentration. The resulting curves for the interhelix interaction free energy are similar in range and in shape, each showing a minimum near room temperature. Theory is also compared with independent experiments, in particular light scattering and crosslinkability studies at nearly neutral pH and found to be reconcilable with both. Examination shows that: 1) The greater acid stability of $\alpha$-tropomyosin is caused by the augmented short-range interactions of aspartic and glutamic residues over those of the aspartate and glutamate species. 2) With small adjustment in input parameters, the same interhelix interaction free energy explains the full range of data at both pH. 3) An implication of this result is that the interhelix salt bridges, while they may provide enough free energy to assure parallel association of helices near pH 7, make a contribution to the total interhelix interaction that is small compared with the hydrophobic contribution. 4) An alternative extant model, the all-or-none-stages model, disagrees with the recent light scattering data and is difficult to reconcile with the concept of loop entropy.

M-AM-E3 PROTEINS IN ELECTRICAL FIELDS. Michael K. Gilson and Barry Honig, Department of Biochemistry and Molecular Biophysics, Columbia University, 630 West 168th Street, New York, N.Y. 10032

The dielectric constant of aqueous protein solutions is greater than that of pure water. The difference is proportional to the concentration of protein, for low concentrations, and the constant of proportionality is known as the dielectric increment.

Two distinct mechanisms have been proposed to account for this phenomenon, but it is not yet clear to what degree either contributes, or how they interact. It is clear, however, that both theories have neglected effects which arise from a treatment of the protein as a low dielectric region. The chief consequences of such a treatment are to increase the tendency of the protein to orient with an applied field and, on the other hand, to decrease the dielectric constant of the protein solution by displacing highly polarizable solvent from that part of the volume occupied by protein. Two further mechanisms under study have to do with induced pK shifts, and with the flexibility of some ionized side chains.

A better understanding of the dielectric increment could permit dielectric measurements to yield more useful information; for example, accurate values for the internal dielectric constants of proteins. Furthermore, the mechanisms at work here apply as well to proteins in electrostatic fields created by other proteins, and by transmembrane potentials.

[Supported by NIH GM30518]

**M-AM-E4** **THE INFLUENCE OF IONIC STRENGTH ON ACETYLCHOLINESTERASE CONFORMATION: KINETICS OF DEALKYLATION ("AGING") OF ORGANOPHOSPHONYL CONJUGATES.** by Harvey Alan Berman and M.M. Decker, Department of Biochemical Pharmacology, State University of New York at Buffalo, Buffalo, New York 14260.

Dealkylation ("aging") of organophosphonyl-acetylcholinesterase proceeds as a carbonium ion mechanism and is expected to be facilitated by charge delocalization. To gain insight into the conformational requirements underlying this process we have examined the kinetics of aging of cycloheptyl methylphosphono-acetylcholinesterase as functions of temperature, pH, and ionic strength. Aging requires a substantial activation energy (25 kcal/mole), and is facilitated by decreases in pH and ionic strength of the buffer. The ionic strength dependence is **opposite** to that expected for a mechanism predicting charge separation during the transition state. Moreover, the modest shift (<0.3 pH units) observed for the rate-pH profile in the presence of different NaCl concentrations is not compatible with a **direct** influence of ionic strength on the reaction participants, but more consistent with an **indirect** effect on enzyme conformation. Conformation requirements were assessed by examining aging kinetics in the presence of cationic ligands specific for the active center and for topographically remote peripheral anionic sites. Only bisquaternary polymethonium cations, which cross-bridge the distance between the two sites, exhibited the capacity to block dealkylation. The results indicate that aging requires an enzyme conformation distinct from the one achieved in the presence of polymethonium ligands, and provide the first evidence for an influence of ionic strength on AchE conformation. (Supported by grants from the N.I.H. (ES-03085) and the U.S. Army Research Office.)

**M-AM-E5** WATER INTERACTIONS WITH VARYING MOLECULAR STATES OF CASEIN: $^{2}H$ NMR RELAXATION STUDIES. Thomas F. Kumosinski, Helmut Pessen, Steve Prestrelski, and Harold M. Farrell, Eastern Regional Research Center, USDA, Philadelphia, PA 19118.

The caseins occur in milk as colloidal complexes of protein and salts, the casein micelles. Removal of $Ca^{2+}$ is thought to result in their dissociation into smaller protein complexes of submicelles. Variations in $^{2}H$ NMR spin-lattice and spin-spin relaxation rates of water with protein concentration have been measured for casein at various temperatures under both submicellar and micellar conditions. $D_2O$ was used instead of $H_2O$ to elimate cross-relaxation effects. From the protein concentration dependent relaxation rates, the second virial coefficient of the protein was obtained by nonlinear regression analysis. Using either an isotropic tumbling or an intermediate asymmetry model, hydrations, $\bar{\nu}$, and correlation times were calculated for the caseins; from the latter parameter the Stokes radius, R, was obtained. Molecular weights, calculated from R using the Stokes-Einstein relationship and the partial specific volume, were in the range of those published by other investigators for the submicelles. Temperature variations of the hydration and Stokes radius of the casein submicelles were consistent with the notion that hydrophobic interactions are the predominant forces responsible for these aggregates. The same temperature variations of R and $\bar{\nu}$ were observed for casein under micellar conditions. However, the absolute values of both the Stokes radii and hydrations, although greater than those obtained under submicellar conditions, are not in agreement with literature values. The speculation that micelles are aggregates of submicelles is consistent with the hydration and Stokes radius results obtained in this study.

**M-AM-E6** LITHIUM-7,SODIUM-23 AND OXYGEN-17 NMR OF LYSOZYME INTERACTIONS WITH ELECTROLYTES IN SOLUTIONS AND POWDERS. T.S. Lioutas, I.C. Baianu* and M.P.Steinberg, Department of Food Science,University of Illinois at Urbana, *Physical Chemistry Laboratory, 1302 West Pennsylvania Avenue, Urbana, Illinois 61801.

$^{7}Li$,$^{23}Na$ and $^{17}O$ Nuclear Magnetic Resonance (NMR) spectra of lysozyme solutions with sodium and lithium chloride were recorded as a function of concentration at 5.87 Tesla. Changes in the quadrupolar relaxation rate, $R_{2Q}$, with increasing concentrations of $Li^+$ and $Na^+$ were observed at 25°C in order to monitor the interactions of lysozyme carboxyl groups with these two cations. Furthermore, the hydration of lysozyme in the presence of such electrolytes was followed by $^{17}O$ NMR, and correlation times were determined for the $^{17}O$ nuclei located in the hydration shells of lysozyme. These measurements extend recent $^{17}O$ NMR studies of aqueous solutions of lysozyme (1,2). $^{17}O$ correlation times are found to be increased for all water populations by the addition of $Li^+$ in concentrations higher than ~1 millimolar to a 10% (w/v) aqueous solution of lysozyme. Changes in lysozyme conformation and solubility were detected in such electrolyte solutions , and $^{7}Li/^{23}Na$ correlation times,in the presence of lysozyme, were determined from the NMR spectra of these two nuclei.From the dependence of $R_{2Q}$ on NaCl and LiCl concentrations in lysozyme solutions we have determined a maximum of 10.7 moles $Li^+$ bound per mole lysozyme, and 10.5 moles $Na^+$ bound per mole lysozyme,respectively.The molar ratios of lysozyme-bound $Li^+$ and $Na^+$ were strongly dependent on the water activity of these electrolyte solutions, which contradicts the basic assumption of the theory of Bull and Breese (3). There is a clear need for an improved theory of protein interactions with electrolytes in solution.
REFERENCES: 1.Halle,B. et al.(1981).J.Amer.Chem. Soc.,103:500-508; 2.Baianu,I.C. et al.(1984).subm. Biophys.J.; 3.Bull,H.B.& Brrese,K.(1970).Arch. Biochem. Biophys.,137:299-307.

**M-AM-E7** CAVITIES AND INTERNAL BOUND WATERS IN PROTEINS. Alexander A. Rashin and Barry Honig, Department of Biochemistry and Molecular Biophysics, Columbia University, 630 West 168th Street, New York, NY 10032

High packing density of the protein interior has been suggested as a major criterion in protein folding studies [1]. It has been found, however, that at least some proteins contain cavities [2,3]. Therefore, it is important to know how many cavities a protein structure can tolerate and whether or not cavities contain water molecules. We have developed an algorithm which locates the cavities in globular proteins of known crystallographic structure, and predicts the positions of water molecules bound within them. The algorithm treats the entire accessible protein surface as a graph, and then finds all separate, connected subgraphs. The largest subgraph corresponds to the outer surface of a protein, and the smaller ones to cavities. Such cavities have been located and characterized in ~30 proteins studied. Predicted positions of water molecules bound in cavities are within ~1 Å of their experimentally determined positions, where these are known.

Supported by NIH (GM-30518) and NSF1 PCM81-18088.

1. Schulz G.E., & Schirmer, R.H. 1979 "Principles of Protein Structure", (C. Cantor, ed.), Springer-Verlag.
2. Lee, B.K., & Richards, F.M. 1971 J. Mol. Biol. 55, 379.
3. Tilton, R.F., Jr., Kunz, I.D., Jr., & Petsko, G.A. 1984 Biochemistry 23, 2849.

**M-AM-E8** ELECTROSTATIC EFFECTS IN PROTEINS James B. Matthew, Genex Corporation, Science and Technology Center, 16020 Industrial Drive, Gaithersburg, Maryland 20877 A high resolution protein crystal structure provides two key elements needed for the calculation of protein electrostatic interactions: the geometric relationship of all charged atoms and the surrounding and intervening atoms which define the "local dielectric value" for each charge pair. The direct evaluation of D from the crystal structure is difficult as evidenced by the wide range of formalisms which have been applied to electrostatic interactions in proteins. The source of diversity in these calculations is the translation of the structural details of the protein, solvent, and their interface into a Coulombic screening term. Two approaches have been taken; microscopic—where the molecular architecture of the protein and solvent is explicitly taken into account (i.e., atomic positions and polarizabilities) and macroscopic which assigns continuous dielectric values to portions or all of the surrounding space incorporating information derived from protein structures such as proximity to the protein-solvent interface. The electrostatic treatment which incorporates a solvent accessibility modification into the Tanford-Kirkwood discrete charge dielectric boundary algorithm has provided a simple and efficient computational procedure which yields quantitative and qualitative predictions which are in agreement with experimental data. The agreement between prediction and experiment is perhaps unexpected. It is clear, however, that a continuum model with dielectric boundaries which incorporates the effect of a protein solvent interface, as well as the presence and distribution of mobile ions, is preferable to an in vacuo or a uniform continum dielectric model. The introduction of a solvent accessibility parameter apparently modulates the charge interaction energy to an extent which adequately portrays the environmental dielectric effects at the real protein surface. MATTHEW, J.B. and RICHARDS, F.M., BIOCHEM 1982, 21:4989; MATTHEW, J.B. and RICHARDS, F.M., BIOPOLYMERS, December 1984; MATTHEW, J.B., WEBER, P.C., SALEMME, F.R., RICHARDS, F.M. NATURE 1983, 169.

**M-AM-E9** MICROSCOPIC AND MACROSCOPIC MODELS FOR CALCULATIONS OF ELECTROSTATIC ENERGIES IN PROTEINS A. Warshel, S.T. Russell and A.K. Churg, Dept. of Chemistry, University of Southern California, Los Angeles, CA 90089-0482

Various approaches for calculations of electrostatic energies in proteins are analysed and compared. An examination of macroscopic approaches demonstrates that the model of Tanford and Kirkwood, which treats proteins as non polar spheres, is inconsistent with experimental facts. It is also shown that a recent modification of the Tanford-Kirkwood model, using solvent accessibility is inconsistent with basic electrostatic theory[1]. It is then explained why the effective dielectric constant of proteins is large and experimental information about electrostatic interactions in proteins is used to obtain a dielectric function (which can be used in studies of charge-charge interactions)[1]. An examination of microscopic models concentrated on calculations of intrinsic $pK_a$'s in BPTI using the protein structure is described. It is shown that calculations that use only the protein permanent dipoles can underestimate the stabilization of charged groups by up to 50 kcal/mol. It is then shown that only calculations that include the permanent and induced dipoles of the protein and the surrounding water molecules can give reasonable results. An extremely effective model that includes all these factors is described. The protein induced dipoles are simulated by a self consistent iterative approach and the surrounding water molecules are simulated by effective self consistent average dipoles (with average orientations determined from molecular dynamics simulations). This model is shown to provide reliable electrostatic energies for ions and ion pairs in proteins[2].

(1) A. Warshel, S.T. Russell and A.K. Churg, Proc. Natl. Acad. Sci. 81, 4785 (1984).
(2) A. Warshel and S.T. Russell, Quart. Rev. of Biophys. 18 (1985).

**M-AM-E10** A POLARIZATION CHARGE MODEL FOR THE COMPUTATION OF MACROMOLECULAR ELECTRIC FIELDS.

R.J. Zauhar, R.S. Morgan, P.B. Shaw, Departments of Biochemistry, Microbiology, Molecular and Cell Biology, and Physics, Pennsylvania State University, University Park, PA

Current calculations of electrostatic interactions in macromolecules involve either the classical method of Tanford and Kirkwood (1), or the method as modified by Shire, et al. (2). Both involve a solution of Poisson's equation within a spherical boundary, and do not preserve the true geometrical relationships of charged sites in a protein. As a consequence, the molecular electric field cannot be computed in a meaningful way by either approach. We present an alternative model based on a representation of solvent dielectric effects by simple distributions of induced polarization charge (3). The model involves the static accessibility of charged sites, and physically reproduces important features of the modified classical method, while maintaining the spatial relationships of charged groups. The macromolecular electric field may now be visualized. Applications to the study of titration behavior will also be presented.

1. J.A.C.S (1957) 79, 5333. 2. Biochemistry (1974) 13, 2967.

3. Zauhar, Morgan and Shaw, Biophysical Journal Feb. 1984, p. 252a.

**M-AM-F1** EFFECT OF PARTIAL EXTRACTION OF TROPONIN ON THE RELATIVE TENSION-PCa RELATION IN SKINNED SKELETAL MUSCLE FIBERS. Richard L. Moss, Julie D. Allen, Gary G. Giulian and Marion L. Greaser, Dept. of Physiology and Muscle Biology Laboratory, Univ. of Wisconsin, Madison, WI 53562.

Last year we showed that partial extraction of troponin-C caused a reversible decrease in the Ca-sensitivity of tension development (BJ45:344a), suggesting that during contraction there are cooperative interactions among adjacent functional groups along the thin filaments. We have further tested this hypothesis by performing experiments in which a small proportion of whole troponin complexes (Tn) were extracted, thereby causing a Ca-insensitive activation of associated functional groups. Tension was measured in solutions containing maximal and submaximal levels of free $Ca^{2+}$: (1) in control fiber segments, (2) in the same segments following partial extraction of Tn, and (3) following recombination of Tn. Troponin was removed from the segments by incubation with $LC_2$ (which apparently contained protease activity) from rabbit soleus muscle and was verified by SDS-PAGE of the fiber segments. Partial removal of Tn resulted in increases in resting tensions to values as great as 0.4 $P_o$, with a concomitant decrease in maximal Ca-activated tension. The relative tension-pCa relation was shifted to higher pCa's by as much as 0.3 pCa unit following Tn extraction, both when tension was measured as total active tension or only as the Ca-sensitive component. Readdition of Tn to the fiber segments resulted in recovery of resting tension to control values and in the return of the tension-pCa relation to its original position. Thus, continuous Ca-insensitive activation of randomly spaced functional groups increased the Ca-sensitivity of tension development in the remaining functional groups. These results further support the idea that there are cooperative interactions among functional groups. (Supported by grants from NIH and the AHA).

**M-AM-F2** RATES OF FORCE REDEVELOPMENT IN SINGLE SKINNED FIBERS FROM FAST-, SLOW-TWITCH AND MIXED MUSCLES OF HAMSTER: A STUDY OF THE CORRELATION WITH $V_{MAX}$ OF SHORTENING. Jagdish Gulati and Aravind Babu, Albert Einstein College of Medicine, Bronx NY 10461.

The study characterizes the rate-limiting step for force development in various muscles, and addresses the question whether this step in the cross-bridge cycle is different from or the same as the rate-limiting step for $V_{max}$ of shortening. Skinned fibers from psoas (fast-), soleus (slow-twitch) and flexor (mixed) muscles were activated with pCa3 at 15°C in a solution containing: (mM) 100 KCl, 4.41 $MgCl_2$, 20 imidazole, 5 ATP, 5 EGTA, 10 CP, 250 units/ml CPKinase and 7.57 $CaCl_2$ (ionic strength 180, pH7). A series of double-step slack releases were imposed during the force plateau, each double-step being followed by a stretch back to the original length (SL=2.5 μm). The first length step was for determining the speed of unloaded shortening $V_{max}$. The force response following the stretch after each double-step was analyzed for the rate-limiting step for force. Sr-activation plots were made for each fiber. The rate constant for force redevelopment was found as 10.2 $sec^{-1}$ (range: 7.3-12.6; see also, Brenner, Biophys J., V45, 1984) for psoas, and 4.1 $sec^{-1}$ (range: 3.5-5.0) for soleus. Flexor fibers had a 10-fold range in speed, but the Sr-response was found to be either of F- and S-types (Gulati, Scordilis & Babu, this Vol.). All the F-type flexor fibers had a force rate-constant of (mean) 9.2 $sec^{-1}$ irrespective of the $V_{max}$ value. The rate-constant of the S-type fiber was 3.3 $sec^{-1}$. The results show (1) that the characteristic rate-constant for force redevelopment and, therefore, the rate-limiting step for force in fast-twitch-type fibers is nearly 3-fold higher than in slow-twitch fibers. (2) The rate-limiting step for force in each fiber-type in the mixed muscle is independent of $V_{max}$, which is evidence that the rate-limitations for force and speed occur at different steps in the cross-bridge cycle. (Supported by NSF and NIH).

**M-AM-F3** FORCE RESPONSE TO ISOMETRIC QUICK RELEASE IN TRABECULAE FROM RAT HEARTS WITH MOSTLY V1 OR MOSTLY V3 VENTRICULAR ISOMYOSIN. Michael Roy Berman and Cynthia C. Lord (Intr. by R.Z. Litten, III). Department of Physiology and Biophysics, University of Vermont, Burlington, Vermont 05405.

The heart can adapt to stress by changing its ventricular myosin isoenzyme pattern. Differences in myocardial performance are correlated with changes in isomyosin pattern, and might be explained by an isomyosin dependent change in the interaction of myosin with actin. To explore this, force transients in response to isometric quick releases were measured in right ventricular trabeculae from rat hearts with mostly V1 or mostly V3 isomyosin. Trabeculae with mostly V1 isomyosin were taken from hearts of normal Sprague Dawley rats; trabeculae with mostly V3 isomyosin from hearts of rats which had 0.8 mg/ml propylthiouracil (PTU) added to their drinking water for 28 days. Trabeculae, mounted between a displacement generator and a force transducer, were chemically skinned, then activated (pCa 5) in an isometric contraction. At the force plateau 8 identical rapid (2 ms) small amplitude (<0.5% muscle length) length releases were applied at 5 second intervals. The force response to each release was digitally sampled (1 kHz rate); the 8 responses were averaged. The averaged response was corrected for the characteristics of the force transducer. A single exponential was fit to the initial 128 ms of the corrected response. Rate constants measured in normal trabeculae (99.9±22.1 $s^{-1}$, n=12) were statistically different (P<.01) than those measured in trabeculae from PTU treated rats (50.7±9.4 $s^{-1}$, n=10). These results suggest that the force generating interaction between myosin and actin is influenced by the isoform of ventricular myosin present in the muscle. Supported by PO1-HL-28001-02/P4.

M-AM-F4 THE VELOCITY OF UNLOADED SHORTENING IN PERMEABILIZED RABBIT FIBERS OF DIFFERENT MYOSIN ISOENZYME COMPOSITION. H.L. Sweeney, M.J. Kushmerick, K. Mabuchi, J. Gergely and F.A. Sreter. Depts. of Radiology, Physiol. and Biophys., Anaesthesia, and Biol. Chem., Harvard Med. Sch.; Depts. of Neurology and Anaesthesia, Mass. Gen. Hospital; and Dept. Muscle Res., Boston Biomed. Research Inst., Boston, Mass.

The slack test was utilized to estimate the velocity of unloaded shortening (pCa 4.3, 12°C) in permeabilized rabbit fiber segments from four different muscles. The myosin was subsequently extracted from segments of these fibers and subjected to pyrophosphate gel electrophoresis. Mean velocities of unloaded shortening ($V_{us}$) were as follows: psoas IIB fibers, 2.20 fiber lengths/s (fl/s) (n=15); tibialis anterior IIB fibers, 1.41 fl/s (n=8); IIA fibers from tibialis anterior resulting from chronic stimulation (cf. Mabuchi et al., Am. J. Physiol., 242, 373,'84), 0.86 fl/s (n=10); vastus intermedius type IIA fibers, 0.82 fl/s (n=5); soleus type I fibers, 0.50 fl/s (n=5). Differences between the isozyme patterns of the psoas and tibialis IIB fibers are indicative of differences in both light chain distribution and heavy chain structure. The vastus and tibialis IIA fibers displayed identical gel patterns that differed from either of the IIB types. The soleus gel pattern showed the presence of the distinct slow type heavy chain. These data suggest that there is a continuum of shortening velocities in skeletal muscle fibers corresponding to the distribution of various light- and heavy chain-determined myosin isozymes. (Supported by grants from NIH - GM15904, AM32018, HL5949, HL23967 - NSF, and MDA)

M-AM-F5 SHORTENING VELOCITY OF SINGLE FIBERS FROM MAMMALIAN SKELETAL MUSCLE DURING DEVELOPMENT. Marion L. Greaser, Peter J. Reiser and Richard L. Moss, Department of Physiology, Univ. of Wisconsin, Madison, WI 53706.

The velocity of unloaded shortening ($V_{max}$) was measured by the "slack test" using single fibers from glycerinated bundles of psoas and EDL muscles from rabbits ranging in age from postnatal day 7 through 14 months. Sarcomere lengths were adjusted to between 2.50 and 2.60 μm prior to inducing slack. The length steps during the slack test usually resulted in sarcomere lengths between 2.00 and 2.24 μm. $V_{max}$ was measured under conditions in which the fibers were maximally Ca-activated at 15°C. The results indicate that single fibers from these two muscles, which are fast-twitch in the adult, undergo identical developmental changes during the period studied. Secondly, $V_{max}$ already has a value at 1 month which is very similar to the value in adult fibers. At postnatal day 7, fibers from both muscles have a mean $V_{max}$ which is significantly lower than that at 1 month. This result suggests that between day 7 and 1 month there are changes in the type of myosin present in these fibers. Thirdly, there is more variation in $V_{max}$ among day 7 fibers than at the other ages studied suggesting that this is a period of transition for maturation of rabbit skeletal muscle. For 10 of 11 fibers from one 7 day psoas muscle, $V_{max}$ was highly correlated (r=0.984) with the tension generating ability for each fiber. This result suggests that as more myosin is incorporated into the contractile apparatus at this age, it is of the fast type. Biochemical data reported by others indicates that this is, in fact, a period of rapid increase in myofibrillar protein synthesis. Preliminary results using SDS gel electrophoresis indicate the presence of two types of myosin heavy chain in neonatal day 1 psoas muscle compared to the single heavy chain observed in the adult muscle. Supported by NIH.

M-AM-F6 FORCE GENERATION DURING SHORTENING AT HIGH VELOCITIES IN THE SOLEUS MUSCLE OF THE RAT. Dennis R. Claflin and John A. Faulkner. Bioengineering Program and Department of Physiology, University of Michigan, Ann Arbor, MI 48109.

In single skeletal muscle fibers, the velocity of unloaded shortening (Vo) determined by the slack test is not different than the velocity of shortening at zero load (Vmax) extrapolated from velocities measured during isotonic releases. In whole soleus muscles of rats, Vo is 60% greater than Vmax (Biophys. J. 45:349a, 1984). This discrepancy has been attributed to the heterogeneity in intrinsic shortening velocity among the fibers of the soleus muscle, with Vo representing the fastest fibers. We tested the hypothesis that during controlled, constant velocity shortening, the minimum velocity at which zero force is generated (Vo') is not different from Vo. Vmax, Vo, and Vo' were determined in vitro at 20°C for each of 10 soleus muscles isolated from 4 week old female rats. Vmax was extrapolated from a hyperbola fitted to 13 velocities measured during isotonic releases. Loads ranged from 5% to 50% of maximum isometric force. Vo was determined from 6 unloaded shortening time intervals. Step releases ranged in amplitude from 7% to 12% of fiber-length. Vo' was determined by measuring force during a series of constant velocity releases. Velocity was increased from 40% of Vmax in increments of Vmax/10 until no further decrement in force was detected. Results in fiber-lengths/s: Vmax = 3.0±0.1; Vo = 5.0±0.1; and Vo' = 4.9±0.1 (means ± S.E.M.). The results support our hypothesis ($p > 0.05$). We conclude that, in the very low load range, force-velocity measurements from heterogeneous skeletal muscle preparations do not lie on the hyperbola fitted to velocities measured during isotonic releases but follow a more sharply curved path which intersects the velocity axis at Vo, not Vmax. (USPHS Grant NS17017.)

**M-AM-F7** TIME-RESOLVED X-RAY DIFFRACTION STUDIES OF MUSCLE ACTIVATION AND CONTRACTION

H.E. Huxley*, M. Kress and R.M. Simmons**. *MRC Laboratory of Molecular Biology, Cambridge, England, and **MRC Cell Biophysics Unit, London, England.

Measurements of the time course of the increase of intensity on the second actin layer-line have shown that it takes place earlier after the stimulus than any of the other changes in the X-ray pattern which we had previously observed and that it is reversed earlier during relaxation. We have interpreted these changes in terms of a troponin-tropomyosin based activation mechanism in the thin filaments which regulates crossbridge attachment and other steps in the crossbridge cycle. In twitches at 14°C the intensity is already decreasing while tension is still rising, again suggesting an activation-related change. We have now found that one component of the increased intensity of the 59Å actin layer-line has a similar time course, whereas a second component, presumably arising from crossbridge attachment rather than activation, has a time course more closely related to tension development. Thus structural changes may take place in actin itself during activation, prior to interaction with myosin.

Observations of the behaviour of the equatorial reflections during small (~1%) but very rapid releases of a contracting muscle show almost no measurable intensity change although a significant increase in spacing takes place, probably arising from the removal of a lateral force component. Some change in structure probably masks the intensity change that would be expected to accompany the spacing change. Tilting of the crossbridges could give this effect for certain types of model, but other structural rearrangements within the myosin head are also possible.

**M-AM-F8** THE EFFECT OF PHOSPHATE (Pi) ON CROSSBRIDGE KINETICS IN PSOAS FIBERS INDICATES THAT THE FORWARD CYCLING RATE INCREASES WITH Pi. M. Kawai, C. Wolen, and T. Cornacchia. Department of Anatomy and Cell Biology, Columbia University, New York, N.Y. 10032

Chemically skinned single fibers are prepared from rabbit psoas, and subjected to maximal activation at pCa 5 and 5mM MgATP. The experiments are carried out in the presence of varying concentrations of Pi (0-16mM) at a constant ionic strength (200mM), and the fibers are subjected to length alterations (sinusoidal or step) during maximal activity. From the transient tension time courses, three exponential processes (A), (B), (C) are identified and plotted against Pi concentrations. The effect of Pi is most striking on process (B) which is responsible for oscillatory work production. Both magnitude B and the rate constant $2\pi b$ increase with Pi concentration, and the plot of oscillatory work output ($\propto Bb$) vs. Pi shows a saturation curve with a $K_m$ of about 3mM. This general conclusion is not altered when the peak-to-peak oscillation amplitude is changed in the range of $0.1\%L_0$ and $0.5\%L_0$. The rate constants and magnitudes of processes (A) and (C) are minimally affected with Pi concentration. Both isometric tension and stiffness (extrapolated to the infinite frequency) decrease gradually with Pi, and the tension to stiffness ratio ($1.2\%L_0$) remains constant. The effect of Pi is different from the effect of ADP: increasing ADP increases isometric tension and decreases rate constants of processes (B) and (C). These observations are consistent with a kinetic scheme where ADP reverses the crossbridge cycle, while Pi accelerates the cycle. Evidently the site of action of Pi on crossbridge cycle cannot be specific to the Pi release step.

**M-AM-F9** THE EFFECT OF STRAIN ON FORCE DECAY FOLLOWING STRETCH OF SKINNED RABBIT PSOAS FIBERS.

Mark Schoenberg and Evan Eisenberg*, NIADDK and NHLBI*, NIH, Bethesda, MD 20205.

Previously (Biophys J. 45:350a:1984), we reported that, in the presence of PPi or AMPPNP, myosin crossbridges in freshly skinned rabbit psoas fibers are not statically bound to actin but exhibit dynamic equilibrium so that the tension produced by a rapid stretch decays to zero as bridges first detach and then quickly reattach to actins in positions of less strain. We showed that for a given condition this decay does not occur with a single rate-constant but rather with rate-constants spanning a wide range. Since the mismatch of myosin and actin helical repeats produces a wide range of crossbridge strain, even at equilibrium, we investigated whether crossbridge strain might influence crossbridge detachment rate. Employing a servo-device capable of maintaining constant sarcomere length, we found that decay of force does not occur over as broad a range of rate-constants as in non-sarcomere length controlled fibers; the rate-constants span just under 2 decades rather than 2-3 decades. The half-times for tension decay remain about the same, ~ 0.2, 1 and 11 s in 4, 1 and 0.25 mM PPi for a 2-nm stretch. To investigate the influence of crossbridge strain, we measured the tension decay following stretches of 1, 2 and 4 nm/half-sarcomere in 1 mM PPi. We found that the half-time for tension decay was ~ 10-fold shorter for 4-nm stretches than for 1-nm stretches. This suggests that variability of crossbridge strain could be a significant factor in producing the wide span of force decay rate-constants. Since the half-times for force decay depend upon [PPi], the effect of increased strain could be due either to an increased rate of PPi binding or an increased rate of crossbridge detachment. Other factors contributing to the wide range of force decay rate-constants could be differences in detachment rate for single-headed and double-headed crossbridges, or the difficulty of some bridges in finding suitable, unoccupied sites in positions of less strain.

**M-AM-F10** MAGNESIUM ION-DEPENDENT STIFFNESS OF RABBIT PSOAS SKINNED FIBERS IN CALCIUM-FREE LOW IONIC STRENGTH SOLUTION: FURTHER EVIDENCE FOR CROSS-BRIDGE ATTACHMENT IN THE RELAXED FIBER. Jagdish Gulati and Aravind Babu. Albert Einstein College of Medicine, Bronx NY 10461.

The skinned fibers make force in the absence of $Ca^{2+}$ in low ionic strength (LIS) in a temperature dependent manner, but the fibers are relaxed at high $Mg^{2+}$ as well as at low temperature (Gulati: Biophys. J. 44, 113, 1983). In the fiber relaxed by low temperature in LIS there is also data suggesting that the cross-bridges are still attached (e.g. Brenner, Yu & Podolsky: Biophys. J. 46, 299, 1984), evidently in a zero force configuration. To study the $Mg^{2+}$-effect, we now examine the stiffness of the relaxed fiber in LIS at both low (0°C) and high (15°C) temperatures. The standard LIS solution was of 40mM ionic strength with free $Mg^{2+}$ varying between 20μM and 10mM. The stiffness measurements were made for stretches of 0.5% to 2.5% Lo at speeds of 2Lo/sec to 50Lo/sec. At 0°-2°C stiffness of the relaxed fiber in 20μM $Mg^{2+}$ was comparable to rigor, and in the 4 to 7 mM $Mg^{2+}$-range the stiffness decreased to a final level of 40% to 60% rigor value. Raising free $Mg^{2+}$ to 10mM had no further effect. The apparent stiffness in 10mM $Mg^{2+}$ was lower (40%) at 2.5Lo/sec rate of stretch than with 50Lo/sec (60%), indicating that much of the $Mg^{2+}$ effect was to increase the exchange rate between attached and detached bridges, rather than to block attachment. The effect of 10mM $Mg^{2+}$ on stiffness was the same at 15°C at 0°C. The results suggest that $Mg^{2+}$ inhibits the $Ca^{2+}$-free force in LIS by blocking the transition from the zero-force configuration (weakly attached bridge; see, Stein, Chock & Eisenberg: Biochemistry 23, 1555, 1984) to high-force, in the turnover cycle. In addition, the results show that $Mg^{2+}$ accelerates the attachment-detachment exchange of the weak bridges. (Supported by National Science Foundation and National Institutes of Health).

**M-AM-F11 MECHANICS OF MUSCLE CONTRACTION AND RELAXATION IN ε-ATP AND CAGED ε-ATP** J.A.Dantzig, D.R.Trentham* & Y.E.Goldman, Dept. of Physiology, Univ. of Penna., Phila., PA 19104, USA and Natl. Inst. for Med. Res.*, Mill Hill, London NW7 1AA, England.

We studied the cross-bridge cycle in the presence of $1,N^6$-etheno ATP (ε-ATP), a fluorescent analog of ATP which supports muscle contraction (Mowery, BBA *159*:374, 1973) and a low level of actomyosin ε-ATPase (Rosenfeld & Taylor JBC *259*:11920, 1984). Glycerol-extracted single fibers from rabbit psoas muscle were put into rigor and then relaxed by laser pulse photolysis of caged ε-ATP. The rise in tension, indicating transient active cross-bridge reattachment with caged ATP (Goldman, et al. J. Physiol.,*354*:577, 1984), was markedly suppressed with caged ε-ATP (Inset). Stiffness, 90° out-of-phase with a 500 Hz, 1 μm length change, was reduced to 17±3% (SEM, n=6) of its value after caged ATP photolysis. Compared to ATP contractions, at 5 mM ε-ATP, steady active tension was reduced to 49±3% (SEM, n=6), quick tension recovery after an abrupt length decrease was 68±2% (SEM, n=6) and unloaded shortening velocity was decreased. Inorganic phosphate (Pi, 10 mM) neither decreased maximum active tension in ε-ATP, nor accelerated final relaxation after photolysis of caged ε-ATP as occurs with caged ATP (Hibberd, et al. Proc. IUPAB 8th Int. Biophys. Cong.:204, 1984). These results are consistent with a cross-bridge model in which Pi release from AM.ADP.Pi is coupled to the mechanical power stroke. Tension per cross-bridge is low in ε-ATP and this decreased force may be due to reduction of Pi release from AM.ε-ADP.Pi. Supported by NIH grants HL15835 to the Penna. Musc. Inst. and AM00745, and by the MRC (U.K.) and the M.D.A.

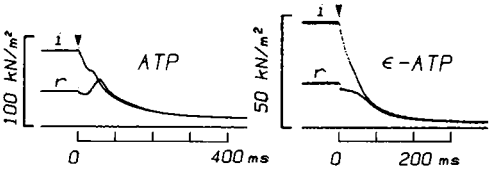


**M-AM-F12** INHIBITION OF MUSCLE CONTRACTION BY THE PRODUCTS OF ATP HYDROLYSIS: ADP AND PHOSPHATE. R. Cooke and E. Pate, Department of Biochemistry and Biophysics, and CVRI, University of California, San Francisco, 94143; Department of Mathematics, Washington State University, Pullman, WA 99164

The products of ATP hydrolysis bind to the nucleotide site of myosin and thus may be expected to inhibit the contraction of muscle fibers. We measured the effects of phosphate and ADP on the isometric tensions and isotonic contraction velocities of glycerinated rabbit psoas muscle at 10°C. Phosphate decreased the force developed in isometric contractions by 30% but did not affect the maximum velocity of shortening ($V_{max}$). The half maximal decrease in force was achieved at 2.8 mM phosphate. Addition of ADP resulted in an increase in isometric tension and a decrease in $V_{max}$. The observed values of $V_{max}$ are described, within experimental accuracy, by a model in which ADP is a pure competitive inhibitor of $V_{max}$ with a $K_i$ of approximately 200 μM. In fatigued fibers, ADP and phosphate levels are known to be elevated, and tension and the maximum velocity of contraction are depressed. The results obtained here suggest that levels of ADP in fatigued fibers are unlikely to play a role in the decrease in function, but that an elevation of the phosphate level is sufficient to account for some of the decrease in tension. This work was supported by grants from the USPHS AM30868, HL32145, from the NSF PCM8208292, and from the Research and Arts Committee of W.S.U.

**M-AM-G1** NEW FLUORESCENT LABELS IN SKELETAL MUSCLE ACTIN AND ACTO-S-1 DISTANCES. Reiji Takashi & Andrzej A. Kasprzak. CVRI, UCSF, San Francisco CA 94143

Dansylcadaverine (DNC) has been tranferred, by transglutaminase from guinea pig liver, to specific glutamine residues of skeletal muscle actin. Degree of labeling levels off asymptotically close to one DNC per actin monomer. Labeling leaves polymerization/depolymerization virtually unaffected, but fluorescence intensity increases 2-3 fold on polymerization. Effect of labeling on interaction with myosin subfragment I (S-1) (studied as $V_{max}$, $K_M^{app}$) is also negligible, and on cross-linking to S-1 with EDC labeled actin produces same "superactivation of S-1 MgATPase" as normal actin. Thus labeled Gln's have no role in foregoing functions. Tryptic digestion of labeled actin [Jacobson, G.R. & Rosenbusch, J.P., Proc. Natl. Acad. Sci. USA (1976), 76, 2742] produces small peptides, some fluorescent, and a non-fluorescent 33 kDa core. Sequence [Elzinga et al., Proc. Natl. Acad. Sci. USA, (1973) 70, 2687] shows that Gln's of proteolyzed 9 kDa region are in range 41-59, i.e., attached DNC(s) are near N-terminus. Distances between label(s) and tetramethyl rhodamine (IATR) attached to "$SH_1$" or to Cys-177 of $LC_1$ of S-1 and 2,4,6-trinitrobenzene sulfonate (TNP) bound to RLR in rigor complex are being estimated by Förster's equation, using energy transfer measurements. All 3 transfers appear to have efficiencies of at least 5-10%. Research supported by HL-16683 and NSF PCM 831-6007.

**M-AM-G2** 5-(IODOACETAMIDO)FLUORESCEIN MODIFIED MYOSIN SUBFRAGMENT-1: A SENSITIVE PROBE TO STUDY THE INTERACTION OF NUCLEOTIDES WITH MYOSIN. Raul Aguirre and Herbert C. Cheung. Department of Biochemistry, University of Alabama in Birmingham, Birmingham, AL 35294

Myosin subfragment-1 (S1) modified at the $SH_1$ with 5-(iodoacetamido)fluorescein (IAF) was used to probe the interaction of subfragment-1 with nucleotides and F-actin. The fluorescence of S1(IAF) decreased about 30% after addition of ADP or ATP. $Mg^{2+}$ per se did not affect the intensity. A similar decrease was also observed upon addition of several polyvalent anions including $SO_4^{2-}$, but at considerably higher concentrations than nucleotides. In the presence of mM $SO_4^{2-}$, nucleotides did not induce further fluorescence decrease. In the presence of 60 mM KCl, 50 mM Tris-HCl, pH 7.7, MgADP bound to S1(IAF) with an apparent dissociation constant of about 1 μM. Association of S1(IAF) to F-actin produced a two-fold fluorescence increase. This enhancement could reversed by addition of MgADP or MgATP in agreement with recent results (Ando, T., Biochemistry (1984) 23,375). The fluorophore in acto-S1(IAF) was more accessible to quenching by iodide than in S1(IAF). Fluorescence decay experiments showed two lifetimes in S1(IAF): A major component of around 0.6 ns and a minor component of 4.2 ns. Rigor formation of S1(IAF) with F-actin shifted the proportions of the two lifetimes in favor of the long lifetime, whereas addition of nucleotides reversed this change. (Supported in part by NIH AM-31239).

**M-AM-G3** THRESHOLD INHIBITION OF S1 ATPase BY PYROPHOSPAHTE. Marsha P. Dale and David D. Hackney. (Intro. by Stephen O'Donnell) Department of Biological Sciences, Carnegie-Mellon Univ., Pittsburgh, PA 15213.

Pyrophosphate is a good competitive inhibitor of the Mg ATPase of S1. By examining the dependence of the rate of ATP hydrolysis upon the pyrophosphate concentration under Vmax conditions, a value for the ratio of the Km of ATP to the Ki of PPi can be obtained. In pH 8 buffer with 30 mM KCl this ratio is 1/2.

When S1 is assayed with pyruvate kinase and PEP (regenerating ATP), a linear increase in ATPase rate is seen on addition of ATP, with a break occurring at the equivalence point of 1 ATP per S1, above which the ATPase rate is constant (Hackney and Clark, Biophys. J. 41, 92a (1983)). In the presence of pyrophosphate, unusual patterns are seen in this assay. For example, with 10 μM S1 and 3 μM PPi there is little inhibition of the ATPase rate at ATP concentrations below 7 μM. This is due to the tight binding of ATP to the excess of PPi-free S1. Above 7 μM ATP, the inhibition is pronounced because ATP must now compete with PPi for the remaining 3 μM S1 sites.

Thus, in this type of a system, the inhibition will reach a maximum value after a critical substrate concentration, then decrease at higher substrate levels.

Supported by grant AM 25980 from the USPHS and by an Established Investigatorship from the American Heart Association to DDH.

**M-AM-G4** THRESHOLD ACTIVATION OF S1 ATPase BY ACTIN AT HIGH S1 LEVEL. David D. Hackney and Patrick K. Clark. Department of Biological Sciences, Carnegie-Mellon Univ., Pittsburgh, PA 15213.

Subfragment-1 (S1), when assayed with pyruvate kinase and phosphoenolypyruvate (PEP) to regenerate ATP, exhibits a linear increase in ATPase rate on addition of ATP until a sharp break occurs at the equivalence point of 1 ATP/active site above which no further increase in ATPase rate occurs (Hackney and Clark, Biophys. J. 41, 92a (1983)). When a similar titration is performed with 6.2 μM S1 in the presence of 1.1 μM actin, there is no activation of the S1 · ATPase by actin as long as the ATP level is below approximately 5 μM. Above 5 μM ATP, however, the rate in the presence of actin increases rapidly and reaches a plateau at 7 μM ATP which is twice the rate for S1 alone. The actin-activated component thus exhibits a threshold effect with no activation below 5 μM ATP switching over to complete activation by 7 μM ATP. Below 5 μM ATP, all the actin will be complexed with nucleotide-free S1 at steady state and the rate will not be activated as no free actin sites are available to stimulate product release from the S1 products complexes. Above 5 μM ATP there will be insufficient nucleotide-free S1 to block the actin sites and activation can occur.

These results are of interest not only to the mechanism of acto-S1, but also as a model system for the study of kinetics at high enzyme concentration.

Supported by grant AM 25980 from the USPHS and by an Established Investigatorship from the American Heart Association to DDH.

**M-AM-G5** ADP DISSOCIATION FROM ACTOMYOSIN-S1 IS SUFFICIENTLY SLOW TO LIMIT THE UNLOADED SHORTENING VELOCITY IN VERTEBRATE MUSCLE. Raymond F. Siemankowski, Meganne O. Wiseman and Howard D. White, Dept. of Biochemistry, University of Arizona, Tucson, AZ 85721.

The rate constant for dissociation of ADP from actomyosin-S1 has been measured in this laboratory (Siemankowski, R. F. and White, H. D. (1984) J. Biol. Chem. 259, 5045-5053) and elsewhere (Marston, S. B. and Taylor, E. W. (1980) J. Mol. Biol. 139, 573-600) for a variety of vertebrate muscle types. We have made the following observations: 1. In solution, the dissociation of ADP from actomyosin-S1 limits the rate of dissociation of actomyosin-S1-ADP by ATP and presumably also limits the rate of crossbridge detachment in contracting muscle. 2. For muscle types in which the rate of ADP dissociation from actomyosin-S1 is slow enough to measure using stopped-flow methods, the rate constants are nearly the same as the theoretical value for the minimum allowable rate constant for dissociation of an attached crossbridge, $k_{min} = V_o \cdot S_L/d$ ($V_o$ is the unloaded shortening velocity in muscle lengths/sec, $S_L$ is the half sarcomere length, and d is maximum crossbridge extension). Therefore, ADP dissociation is sufficiently slow to be the molecular step that limits the maximum shortening velocity of these muscles. 3. Variation with muscle type of the rate constant for ADP dissociation may be a general phylogenetic mechanism for regulating shortening velocity.

This work has been supported by research grants from the Arizona Heart Association, Muscular Dystrophy Association and HL20984.

**M-AM-G6** KINETIC MECHANISM OF 1,$N^6$ ETHENO-aza-ATP AND 1,$N^6$-ETHENO-aza-ADP BINDING TO CARDIAC ACTOMYOSIN-S1 AND MYOSIN-S1. Susan J. Smith and Howard D. White, Dept. of Biochemistry, University of Arizona, Tucson, AZ 85721.

The fluorescence emission of 1,$N^6$-etheno-2-aza-ATP (ε-aza-ATP) is enhanced approximately three-fold and shifted from 485 nm to 460 nm during steady state hydrolysis by bovine cardiac myosin-S1 and actomyosin-S1. The time course of nucleotide fluorescence enhancement observed during ε-aza-ATP hydrolysis by myosin-S1 and actomyosin-S1 is qualitatively similar to the time course of tryptophan fluorescence enhancement observed during ATP hydrolysis: 1) A rapid increase to a maximum level is observed upon the addition of ε-aza-ATP. 2) The nucleotide fluorescence slowly decreases to a final level, which is about 30% the maximum enhancement; a similar fluorescence enhancement is obtained by adding ε-aza-ADP to myosin-S1 or actomyosin-S1 under the same conditions. The apparent second order rate constants of ε-aza-ATP binding to cardiac myosin-S1 ($2x10^5$ $M^{-1}s^{-1}$) or actomyosin-S1 ($4x10^5$ $M^{-1}s^{-1}$) are 5-10 times slower than those for ATP. The rate at which ε-aza-ADP dissociates from cardiac myosin-S1 is 1.9 $s^{-1}$ under the same conditions. In the presence of actin, the rate constant of ε-aza-ADP dissociation from cardiac myosin-S1 is 110 $s^{-1}$ at 15° C; this can be compared to the rate constant of ADP dissociation from bovine cardiac actomyosin-S1, 70 $s^{-1}$ under similar conditions.

Although there are quantitative differences between the rate and equilibrium constants of ε-aza and adenosine nucleotide binding to cardiac actomyosin-S1 and myosin-S1, the basic features of the mechanism are unchanged. Experimental conditions: 100 mM KCl, 10 mM MOPS, 5 mM $MgCl_2$, 0.1 mM DTT, pH 7.0, 15° C. This work was supported by research grants from the Muscular Dystrophy Association, Arizona Heart Association, HL 20984, and a British American Heart Association fellowship to SJS.

**M-AM-G7** THE KINETIC MECHANISM OF 1,$N^6$ ETHENO-2-aza-ATP AND 1,$N^6$ ETHENO-aza-ADP BINDING TO BOVINE CARDIAC ACTOMYOSIN-S1 AND MYOFIBRILS. Susan J. Smith and Howard D. White, Dept. of Biochemistry, University of Arizona, Tucson, AZ 85721.

The fluorescence emission of 1,$N^6$ etheno-2-aza-ATP (ε-aza-ATP) is enhanced approximately three-fold and the emission maximum is shifted from 485 to 460 nm during steady-state hydrolysis by cardiac actomyosin-S1 and myofibrils. The large change in nucleotide fluorescence at 410-460 nm has been used to make kinetic measurements of ε-aza-ATP binding to and ε-aza-ADP dissociation from cardiac actomyosin-S1 and myofibrils in a front-face, stopped-flow fluorescence cell. At concentrations of ε-aza-ATP >20 μM, the kinetics of ε-aza-ATP binding are clearly biphasic for both actomyosin-S1 and myofibrils. The rate of the more rapid phase of the fluorescence transient is proportional to nucleotide concentration and can be described by a second order rate constant of $\sim 1 \times 10^5 M^{-1}s^{-1}$, whereas the rate of the slower phase, $2\text{-}3 s^{-1}$, is essentially independent of nucleotide concentration. The kinetics of the dissociation of bovine cardiac actomyosin-S1 by ε-aza-ATP, measured by light scattering are also biphasic and can be described by the same set of rate constants as those for nucleotide binding. The rate constants of dissociation of ε-aza-ADP from bovine cardiac actomyosin-S1 and myofibrils, measured from the decrease in fluorescence of the bound ε-aza-ADP upon displacement by ATP, are 18 and 20 $s^{-1}$, respectively at 0° C. These results suggest that the geometric constraints imposed on the interaction of actin and myosin by the three dimensional structure of the myofibril do not modify the kinetics of ε-aza-ATP binding or ε-aza-ADP dissociation. Experimental conditions: 100 mM KCl, 10 mM MOPS, 5 mM $MgCl_2$, 0.1 mM DTT, 0.1 mM EGTA, pH 7.0, 0° C. This work was supported by research grants from the Muscular Dystrophy Association, AZ Heart Association, HL 20984, and a British-American Heart Association Research Fellowship to SJS.

**M-AM-G8** EFFECT OF C-PROTEIN ON CARDIAC MUSCLE ACTOMYOSIN ATPase. H. Criss Hartzell (Intr. by L. J. DeFelice) Anatomy Dept., Emory University School of Medicine, Atlanta, Ga. 30322

C-protein, a component of thick filaments of striated muscles, is reversibly phosphorylated and dephosphorylated in heart. C-protein may be involved in regulating contraction because the extent of C-protein phosphorylation correlates with the rate of relaxation of the cardiac contraction (J. Gen. Physiol. 83: 563, 1984). To test this hypothesis, we examined the effect of C-protein purified from chicken heart on actin-activated cardiac myosin ATPase. The ATPase velocity was measured by hydrolysis of $^{32}$P-ATP in 10 mM citrate-Tris buffer, pH 8. With [myosin] = 0.65 μM, 20 μM actin activated the myosin ATPase ~20-fold. The effect of C-protein on actomyosin ATPase was concentration-dependent. Above 3 μM C-protein, ATPase activity was depressed (>75% inhibition at [C-protein] =10 μM), whereas C-protein concentrations of 1 - 0.1 μM stimulated ATPase activity 1- to 2-fold. To determine the kinetic mechanism of the stimulation, ATPase activity was examined as a function of actin concentration (10-60 μM). In the absence of C-protein, $V_{max}$ = 0.16/sec and $K_m$ = 3.0 μM. In the presence of 0.8 μM unphosphorylated C-protein (<0.2 mol phosphate per mol C-protein), $V_{max}$ was increased to 0.3/sec, but $K_m$ was unchanged (3.4 μM). At optimal [C-protein], the stimulatory effect of C-protein was dependent upon the molar ratio of C-protein to myosin, with maximal effects occurring at C-protein/myosin >1. C-protein had no effect on the $Mg^{2+}$, $Ca^{2+}$, or $K^+$-EDTA ATPase activities of myosin in the absence of actin. It is suggested that the stimulatory effect of C-protein occurs as a result of cross-linking thick and thin filaments such that filaments are in better register and more myosin heads are favorably oriented to interact with a thin filament. The significance of this observation to cardiac relaxation is discussed. (Supported by NIH HL 21195)

**M-AM-G9** LIGAND EFFECTS ON ACTO-S1 ATPASE OF CARDIAC MYOSIN ISOZYMES. Joseph Rivera and Paul Dreizen. Biophysics Graduate Program, SUNY Downstate Medical Center, Brooklyn, N.Y.

Atrial and ventricular myosins have different light and heavy chains. We have investigated the steady-state acto-S1 ATPase of these two isozymes from canine cardiac muscle. Vmax is about 3 times greater for atrial than ventricular S1, and Km is roughly 3 times stronger for ventricular than atrial S1. In previous studies on rabbit fast muscle myosin isozymes, Balish and Dreizen (1984) have shown that ligand effects on acto-S1 ATPase are not simply related to ionic strength, but can be attributed to highly specific interactions at a small number of anionic and $Mg^{++}$ binding sites, and that light chain isozymes exhibit significant differences in their ligand sensitivities. The cardiac S1 isozymes show the same general features as in rabbit fast muscle isozymes. ATP and monovalent anions act as potent competitive inhibitors of acto-S1 ATPase. This effect involves multiple binding sites, probably 3 sites, and inhibition constants (Ki) are strongest in the order $ATP \gg SCN^- > Cl^- > Ac^-$. $MgCl_2$ is also a multisite competitive inhibitor of acto-S1 ATPase, but this appears to involve joint, independent contributions from a single $Mg^{++}$ site and multiple $Cl^-$ (anionic) sites. The ligand inhibition constants are significantly greater for ventricular S1 than atrial S1. For example, Ki values for ATP inhibition are about 1.2 mM for ventricle and 2.5 mM for atrial myosin S1, and the Ki values for $Cl^-$ inhibition vary from 20 mM (ventricular S1) to 40 mM (atrial S1). Although Vmax and Km values are different for cardiac and fast muscle isozymes, the ligand inhibition constants are similar for ventricular S1 and fast muscle S1-LC1, and also for atrial S1 and fast muscle S1-LC3. Thus, stronger ligand inhibition constants are found for the isozymes with light chains that contain the excess peptide sequence at the N-terminal end (ventricular S1 and fast muscle S1-LC1).

M-AM-G10 ETHYLENE GLYCOL HYBRIDIZATION OF FAST SKELETAL AND SMOOTH MUSCLE MYOSINS - LIGHT CHAIN EXCHANGE. S. P. Scordilis Dept. Biol. Sci., Smith College, Northampton, MA 01063.

A new protocol has been devised which allows for the hybridization of any myosin light chain (alkali or P-light chains) with another heavy chain isoform. The method involves the incubation of column purified myosin with a 10 fold molar excess of purified homologous light chains in a solution of 36% deionized ethylene glycol, 600 mM KCl, 16 mM EDTA, 9 mM MgATP, 6 mM Tris-HCl (pH 7.0) and 0.1 mM DTT. This mixture was gently stirred for 90 min at 25°C. The exchange reaction was terminated by dialysis against saturated $(NH_4)_2SO_4$ and 10 mM EDTA. The insoluble hybridized myosin was pelleted at 45,000 x G for 20 min. The pellet was resuspended in a high ionic strength buffer and chromatographed on Sepharose Cl-4B to remove any contaminating light chains. SDS PAGE demonstrated that between 50% to 75% of the light chains were exchanged in rabbit fast skeletal muscle myosin with bovine abomasal smooth muscle light chains. The high ionic strength ATPase activities were identical in the control rabbit skeletal muscle myosin and in the smooth muscle light chain containing hybrid in the presence of EDTA, $Ca^{2+}$ or $Mg^{2+}$. The actin-activated low ionic strength Vmax or Kapp (actin) appear to be somewhat altered in the the hybrid. In short, both smooth muscle light chain types have been exchanged into the fast skeletal muscle myosin heavy chains. This smooth/skeletal muscle hybrid demonstrated no change in the characteristic high ionic strength ATPase activity values, but may exhibit some change in the actin-activated activity.

This work was supported by grants from the Muscular Dystrophy Association of America and the Blakeslee Fund for Genetics Research at Smith College.

M-AM-G11 MYOSIN ISOZYMES IN SINGLE FIBERS FROM FROG SKELETAL MUSCLE. E.D. Pagani, R. Faris, S. Striz, F.J. Julian, Dept. of Anesthesia Research, Brigham & Women's Hospital, Boston, MA.

Intact fibers from the iliofibularis muscle of the frog (Rana temporaria) have been classified as "fast twitch" or "slow non-twitch" based on their contractile properties. In the presence of acetylcholine, fast twitch fibers contract then relax, whereas slow non-twitch fibers remain contracted. Using the above criteria we selected slow non-twitch and fast twitch fibers from the iliofibularis muscle. Myosin from a single fiber of each type (5-12 mm length; 60-100 um diameter) was analyzed by SDS or pyrophosphate polacrylamide gel electrophoresis with modifications (Pagani and Julian, Circ. Res. 54: 586, 1984). All gels were silver-stained using modified versions of the method of Morrissey (1981). SDS gel analysis showed that myosin from a slow non-twitch fiber has two major light chains, whereas myosin from a fast twitch fiber has three major light chains. On pyrophosphate gels, myosin extracts from slow non-twitch fibers showed one or two slowly migrating myosin band (s); however, myosin extracts from fast twitch fibers showed two general patterns both distinct from that of myosin from slow non-twitch fibers. One type of fast twitch fiber showed two or three slowly migrating myosin bands and three fast migrating myosin bands, another type of fast twitch fiber showed only three fast migrating myosin bands. These results suggest that there are differences in myosin among fast twitch fibers as well as between fast twitch and slow non-twitch fibers. This finding may partially explain the range of values for the maximum speed of shortening among intact fast twitch fibers that has been observed in this laboratory. Supported by NIH Grants HL06563 (EDP) and HL30133 (FJJ).

M-AM-G12 COMPARATIVE OXYGEN EXCHANGE STUDIES ON MYOFIBRILS AND MYOSIN FROM MYOPATHIC AND NORMAL HAMSTER HEARTS. Stephanie A. Davidoff, Kamal K. Shukla, and Harvey M. Levy. State Univ. of N.Y. at Stony Brook, Stony Brook, N.Y. 11794

The basic cellular dysfunctions underlying cardiomyopathy are as yet unknown. In an attempt to determine if any of these occur at the level of the basic contractile proteins, we compared the oxygen exchange catalyzed by washed myofibrils and purified myosin from normal and myopathic hamster hearts. This oxygen exchange (between water and the $P_\gamma$ group of myosin-bound ATP) occurs at an intermediate stage in the hydrolysis of MgATP by the muscle proteins, myosin and actin. Our results indicate that myofibrils from the myopathic hearts are associated with a relatively large amount of non-specific phosphatase and this extra phosphatase activity shows up in four ways: 1) the oxygen exchange distribution of the product Pi shows a higher than normal level of unexchanged Pi (which would be expected for a non-myosin phosphatase); 2) there is a higher than normal rate of MgATP hydrolysis in the absence of $Ca^{2+}$ when the contractile proteins are virtually inactive; 3) there is a lower than normal rate of MgATP hydrolysis in the presence of $Ca^{2+}$ when the actin-activated MgATPase of myosin predominates; and 4) there is a higher than normal level of ADPase activity in the myopathic myofibrils. In contrast to these results with myofibrils, there appeared to be no difference between the oxygen exchange properties or the MgATPase activity of purified myosin from normal or diseased hearts. Overall, our results indicate that the actin-activated MgATPase is the same for normal and myopathic hearts, but that the myofibrillar fraction from myopathic tissue, even after extensive washing, contains a larger than normal level of some as yet unidentified phosphatase activity. (Supported by NSF Grant PCM 8211289)

**M-AM-H1** SURFACE PROCESSES IN ION TRANSPORT AND EXCITATION. Martin Blank
Biological Sciences Division, Office of Naval Research, Arlington, VA 22217

Surface processes are critical in ion transport, and we have included them in a description of ion fluxes by treating the electrical double layer regions of membranes as compartments. Standard physical chemical equations describe the effects of surface concentrations, charges, potentials and capacitances on the ion fluxes. In the presence of a non-selective voltage gated channel, we obtain the currents normally observed during a voltage clamp (i.e. early inward currents and later outward currents that are functions of the applied voltage) (Bioelectrochem. Bioenerg. 10:451, 1983). The apparent ion selectivity arises from the normal asymmetry of the resting ionic concentration gradients, but the gating current conductance and the surface capacitance have strong effects on the currents. A decrease in either property can change a sodium selective channel into a potassium selective channel. The opening of the ion channel can also be explained by surface processes, i.e. the effect of surface charge on oligomer association equilibria (Bioelectrochem. Bioenerg. 9:615, 1982). Shifts in the asymmetrically distributed surface charge are brought about by depolarization, and the increased charge can cause local disaggregation (i.e. channel opening). A ligand gated channel may function by the same mechanism, since ligand binding leads to changes in surface charge in some cases.

(This work was performed at Columbia University and supported by contract N00014-83-K-0043 from the ONR.)

**M-AM-H2** HARMONIC ANALYSIS OF PERIODIC GATING CURRENTS IN DYNAMIC-STEADY-STATE. William J. Adelman and Jurgen F. Fohlmeister. Lab. of Biophysics, NINCDS, NIH at the Marine Biological Laboratory, Woods Hole, MA 02543, and Lab of Neurophysiology, Univ. of Minnesota, Minneapolis, MN 55455.

Gating currents were obtained from pronase-treated squid axons under sinusoidal voltage-clamp in the frequency range of 0.5 to 5 kHz. The current records were analyzed as a function of $E_{mean}$ ($-112\ mV \leq E_{mean} \leq +76\ mV$) about which the voltage was varied with an amplitude of ±35 mV. The current records were highly distorted relative to a pure sine wave, and showed a bimodal shape for Emean in the middle and upper end of the gating range (-25 to +40 mV). The second peak, which occurred during the early falling phase of the command sinusoid, becomes increasingly large with increasing $E_{mean}$, and becomes the dominant peak for $E_{mean} \geq +10$ mV. This qualitative pattern was maintained for the full experimental frequency range. The harmonic content of the periodic wave-form is dominated by the second harmonic whose amplitude increases with $E_{mean}$ at a rate that is roughly proportional to $m_\infty^3$ of the Hodgkin-Huxley model as a function of E. For $E_{mean} > +10$ mV the distortions again decline. This behavior is in sharp contrast to simulated gating currents generated by Hodgkin-Huxley model kinetics and simple aggregation gating kinetics among others which are shown to be "dynamically equivalent" among themselves. Kinetics that are dynamically equivalent to the experimental data have been developed. (The records shown at right are for a frequency of 730 Hertz.)

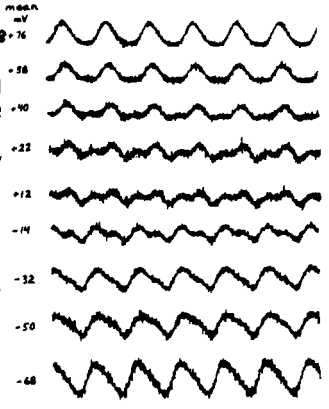

**M-AM-H3** MODEL CONSTRUCTION AND SIMULATION OF GATING CURRENT DATA OBTAINED IN DYNAMIC-STEADY-STATES. Jurgen F. Fohlmeister and William J. Adelman. Lab of Biophysics, NINCDS, NIH at the Marine Biological Lab, Woods Hole, MA 02543 and Lab of Neurophysiology, Univ. of Minn.,Minneapolis MN 55455

Gating current records obtained under conditions of dynamic-steady-state for large-amplitude sinusoidal voltage-changes are interpreted in terms of the kinetics of channel-molecular conformational transitions; the form of the records is periodic and is assumed to be the result of kinetic feedback patterns determined by the overall gating-kinetic scheme. Simulated gating currents generated by "standard" kinetics including those of the Hodgkin-Huxley model and of simple aggregation gating among others were found to be dynamically equivalent and in fundamental disagreement with experimental data. The standard models show a deep minimum in the amplitude of the second harmonic for Emean = -35 mV. In contrast the experimental data show a pronounced and broad peak in that amplitude for $E_{mean}$ = +10 mV. For physical reasons the data were modelled in terms of two kinetic processes that are coupled in such a way that the two processes are sequential and therefore contribute components to the gating current at different phases of the command-sinusoid, as required by the data. Having determined a basic model kinetic structure that yields gating current records that are dynamically equivalent to the experimental records, the rate "constants" are adjusted to fit details of the experimental data. The resulting quantitative model predicts "flickering" in the open state of single channels and sizeable gating currents in the near hyperpolarized region of membrane potentials along with a very weak Cole-Moore type shift for Na-activation gating. Furthermore, the model gives the correct threshold behavior and action potential response when supplemented with Na-inactivation and K-activation processes.

M-AM-H4 THRESHOLD CHANNELS CAN ACCOUNT FOR STEADY-STATE TTX-SENSITIVE SODIUM CURRENT OF SQUID AXON. R.F. Rakowski, Paul De Weer and D.C. Gadsby, Marine Biological Laboratory, Woods Hole, MA.

The TTX-induced change in holding current of internally dialyzed voltage-clamped squid giant axons was measured between -80 and +30 mV. Holding currents were minimized by reducing internal $[K^+]$ from 280 to 140, 70 or 0 mM (N-methylglucamine replaced $K^+$). Internal $[Na^+]$ and external $[K^+]$ and $[Na^+]$ were 50, 10 and 425 mM, respectively. Temperature, 17°C. At all voltages, TTX caused an outward change in holding current, presumably reflecting block of a steady-state inward current through TTX-sensitive $Na^+$ channels. This inward $Na^+$ current was very small near -80 mV, peaked between -30 and -40 mV (maximum inward current -6.4 ± 0.4 μA $cm^{-2}$; 20 measurements on 5 axons) and could be linearly extrapolated to the calculated $Na^+$ equilibrium potential of +54 mV. The data are poorly fit by either the classical Hodgkin-Huxley steady-state equations ($m^3(\infty)h(\infty)$) or Rudy's modification (J. Physiol. 283: 1, 1978) to account for slow inactivation ($m^3(\infty)h(\infty)s(\infty)$). Instead, we find that the data can be adequately fit by a non-inactivating, two-state Boltzmann distribution function in which the fraction of open channels = $1/[1+\exp(V^*-V)Z/25)]$ where V = holding potential, $V^*$ = -52 ± 2 mV and Z = 5.1 ± 1.0; maximum conductance of steady-state open channels was 72 ± 3 μS $cm^{-2}$. These characteristics are very similar to the activation properties of the "threshold channels" recently described by Gilly and Armstrong (Nature 309: 448, 1984). The findings suggest that in the steady state the classical voltage-dependent $Na^+$ channels populate only closed or inactivated states and that the steady-state inward $Na^+$ current can be ascribed to a small population of threshold $Na^+$ channels that undergo incomplete inactivation. Supported by NIH grants NS11223 to P.D.W. and NS19393 to R.F.R.

M-AM-H5 FREQUENCY DOMAIN MEASUREMENTS OF MEMBRANE CAPACITANCE IN SQUID AXONS WITH AND WITHOUT RISING PHASE ON THE GATING CURRENT. Stimers, J.R., Bezanilla, F. and Taylor, R.E. Dept. Physiology, UCLA, Los Angeles, CA, Lab. Biophysics, NINCDS, NIH, Bethesda MD and Marine Biological Laboratory, Woods Hole MA.

Giant axons from the squid Loligo pealei were perfused and voltage clamped by standard techniques. A pseudorandom noise signal was generated by a Lomas Lightning One microcomputer for use in investigating membrane capacitance in the frequency domain. Amplitudes were calculated for 512 discrete evenly spaced frequencies of sinusoidal waves which were then added together in pseudorandom phase. The frequency range is controlled by the rate at which the points are delivered to the preparation. Recordings of membrane current were done under conditions of balanced osmolarity or with the external solution hyperosmotic with respect to the internal solution. Two reasons for these experiments are: 1) to extend the frequency range of measurement to 70 kHz and 2) to check the predictions of our model for the effect of an osmotic gradient across the membrane (Stimers et al., Biophys. J. 45:12a, 1984). The prediction is that the imaginary part of the capacitance should decrease and the frequency at which the imaginary part of the capacitance is maximum should increase when the external solution is made hyperosmotic. Also, an increase in the apparent non-lossy capacitance is expected. Experimentally all of the predictions were found to be true. The maximum imaginary capacitance decreased from about .2 μF to .1 μF and the peak frequency increased from about 15 KHz to 30 KHz. The non-lossy capacitance increased from .6 to .8 μF.

This research was supported by USPHS grant #GM30376 to FB and NIH fellowship to JRS.

M-AM-H6 MULTIPLE EXPONENTIAL COMPONENTS IN THE FALLING PHASE OF SODIUM CURRENT. M. D. Rayner and J. G. Starkus. Bekesy Laboratory of Neurobiology and Department of Physiology, University of Hawaii, 1993 East-West Road, Honolulu, HI 96822.

After careful elimination of possible artifacts due to series resistance errors, periaxonal $Na^+$ accumulation and electrode polarization, multiple exponential components are still readily apparent in the falling phase of sodium current in crayfish giant axons. At positive potentials, the same time constants can be extracted both from single pulse sodium currents and from the envelope formed by the test pulse sodium currents of the standard double pulse protocol used for evaluation of pre-pulse inactivation rate. Using this double pulse protocol we find that the weighting factors (time zero intercepts) of the extracted exponential components, are markedly affected by interpulse interval. For short interpulse intervals ( 300 μs), observed weighting factors are similar to those extracted from single pulse sodium currents. Thus under these conditions the apparent "tau h" is approximately equal to "tau c".

For longer interpulse intervals the weighting factors of the faster components decrease, whereas the slower components of inactivation show progressively larger intercepts. Thus the observed "tau c" departs progressively from "tau h" as interpulse interval is increased, since the early part of the test pulse envelope is increasingly distorted by these slower inactivation components.

**M-AM-H7** IS THE EXCITABLE SODIUM CHANNEL THE MAJOR PATHWAY FOR THE RESTING SODIUM CURRENT?
D. C. Chang, Department of Physiology, Baylor College of Medicine, Houston, TX 77030, and Jessica Liu, Department of Biochemistry, Harvard University, Cambridge, MA 01432.

It is often assumed that the permeability ratio $P_K/P_{Na}$ of a nerve membrane varies with the potential as the conductance ratio ($g_K/g_{Na}$) described in the Hodgkin-Huxley model. If this is the case, then the pathways for the resting current must be the same as the excitable channels. This assumption, however, has difficulties in explaining the finding that tetrodotoxin (TTX), which selectively blocks the sodium channel, has very little effect on the resting potential. If the resting sodium current must pass through the $Na^+$ channel, then blocking this channel should significantly affect the membrane potential.

One possible explanation of this paradox may be that the total amount of sodium current at the resting state could be very small and thus contribute very little to the membrane potential. To test such interpretations, we studied the resting potential of the squid axon and compared the effects of applying TTX with the replacement of external $Na^+$ by impermeable ions (choline). Under $[K]_o$ = 0 situation, we found that TTX hyperpolarizes the axon for less than 1 mV. On the other hand, removal of external $Na^+$ gives a hyperpolarization of over 4 mV. Even when the axon was under the treatment of $4 \times 10^{-7}$ M TTX, which completely blocked the action potential and abolished the voltage-gated sodium conductance, we still observed a hypolarization of 3.8 ± 1.1 mV when the external $Na^+$ was replaced. These observations suggest that the resting $Na^+$ current is carried mainly through pathways different from the excitable $Na^+$ channel.

**M-AM-H8** SUPPRESSION OF SODIUM CHANNEL GATING CURRENT BY EXTRACELLULAR SAXITOXIN AND TETRODOTOXIN w IN CRAYFISH AXONS. J. G. Starkus and S. T. Heggeness. Bekesy Laboratory of Neurobiology and Department of Physiology, University of Hawaii, 1993 East-West Road, Honolulu, HI 96822.

Comparison of gating currents in crayfish giant axons prior to and after external application of either STX or TTX, clearly indicates significant suppression of total gating charge movement. This suppression of $I_gON$ occurs without any visible alteration in the kinetics of charge movement. The effects of external STX on $I_gON$ are concentration dependent, hold potential sensitive, and reversible following washout of toxin. At a hold potential of -90 mV, 1 nM STX was found to produce a 25% suppression of $Q_{ON}$. Increasing the dose of 10 nM STX resulted in a 49% suppression of $Q_{ON}$. Removal of external STX resulted in a near complete recovery of $I_gON$ to control levels (no STX). The suppression of $I_gON$ by external toxin was found to be hold potential dependent, with only minimal suppression observed at the most hyperpolarized hold potentials, -140 to -120 mV. The maximal effect of STX on $I_gON$ was observed at hold potentials where the $Q_{ON}$ vs. $V_H$ plot was found to be the most voltage sensitive, -100 to -80 mV. This suppression of $I_gON$ by STX is partially relieved following removal of normal inactivation by intracellular pronase treatment. These results could be explained if the binding of toxin altered steady state inactivation by shifting its voltage sensitivity by approximately 10 mV.

**M-AM-H9** FOUR LIPID-SOLUBLE TOXINS MODIFY SODIUM CHANNEL GATING. Mark D. Leibowitz, Jeffrey B. Sutro and Bertil Hille, Physiol. & Biophys. Dept., U. of Washington, SJ-40, Seattle, WA 98195.

The alkaloids veratridine and cevadine and the insecticides allethrin and DDT modify gating of Na channels in frog skeletal muscle (~10°C, vaseline gap voltage clamp). Open channels are required for the modification. Modified channels are seen after conditioning depolarizations as tail currents that decay slowly at a holding potential of -90 mV (relaxing with $\tau$ = 3100, 2100, 4.3 and 2.0 ms for veratridine, cevadine, allethrin and DDT respectively. Removing fast inactivation with N-bromoacetamide increases the magnitude of the slow tail current with each toxin, presumably by keeping more channels open long enough to be modified. Toxin-induced tail currents decay much more rapidly during hyperpolarizations. Veratridine and cevadine-modified channels that have been shut this way re-open upon return to -90 mV. We did not see such re-opening of allethrin or DDT modified channels. With alkaloids, closing and opening kinetics are described by sums of two decaying exponentials with voltage-dependent taus. Between -170 and -74 mV the two taus vary between 0.25-2 ms and 6-19 ms. This gating of alkaloid-modified channels is characterized by a 73 mV negative shift in the midpoint of the $I_{Na}$ activation curve (larger than the shift known for batrachotoxin and aconitine). As for normal activation gating, a fivefold increase in external $[Ca^{2+}]$ shifts both the $I_{Na}$ activation curve and the tau vs. voltage relationships for veratridine-modified channels by +12 to +16 mV. In addition changes in the instantaneous I-E relation suggest that $Ca^{2+}$ ions block and permeate modified channels. As judged by the criteria evaluated, the readily available alkaloid cevadine can be substituted for veratridine. Supported by NIH grants NS08174, GM07270, and NS07097 and a US ARO grant for equipment.

**M-AM-H10** Na CHANNEL ACTIVATION SHIFTS AFTER INACTIVATION REMOVAL IN NEUROBLASTOMA CELLS. Tohru Gonoi, Katsuro Ashida, William A. Catterall, and Bertil Hille, Depts. of Pharmacology (SJ-30) and Physiology & Biophysics (SJ-40), University of Washington, Seattle, WA 98195.

Macroscopic Na currents were recorded from N18 neuroblastoma cells by the whole cell method using pipettes containing in mM: 10 Na, 150 Cs, 60 Cl, 100 F (at 15°C). The bath contained mammalian Ringer or solutions with some of the Na replaced by TEA. Stable Na currents could be recorded for over an hour with no fall in amplitude or shift of the midpoint of the activation curve. Inactivation of $I_{Na}$ was nearly eliminated by external 0.2 mM N-bromoacetamide or by internal 0.25 mg/ml trypsin, or α-chymotrypsin, and inactivation was drastically slowed by external 200 nM Leiurus q. toxin or 500 nM Goniopora (coral) toxin. Unlike what has previously been reported in nonmammalian preparations, these treatments increased $I_{Na}$ at all voltages and shifted the midpoint of the activation curve in the negative direction. The shift was not due to a series resistance artifact since diluting the Na to 50 or 33% of normal had no effect. The shift was about -23 or -19 mV with trypsin or NBA, respectively, and about -8 mV with the toxins. The shift considerably increased the size of $I_{Na}$ at low depolarizations. $G_{Na}$ also increased at the large depolarizations (to +30 mV) by about 55 or 35% with trypsin or the toxins, respectively. NBA often reduced $I_{Na}$ some minutes after increasing it. Such shifts and increases of peak $I_{Na}$ are expected for two commonly considered schemes of gating kinetics. They would occur: 1) in a linear rest-open-inactivated scheme with fast and weakly voltage dependent inactivation, and 2) in a branched scheme where channels inactivate from rest with a voltage dependence less steep than activation from rest.
Supported by NSF grant BNS8021619, NIH grants NS08174 and RR00374, and a US ARO grant for equipment.

**M-AM-H11** COMPETITORS OF NA CHANNEL INACTIVATION. Clay M. Armstrong and Richard J. Bookman. Department of Physiology, University of Pennsylvania, Philadelphia, PA., 19104.

Some pharmacological agents, e.g. 9-aminoacridine (9AA) and QX-314, produce a 'use-dependent' block of Na channels when applied to the inside of the membrane. Other agents, e.g. pancuronium and Azure A (AzA), also block from the inside but show no use-dependence. The former are said to promote inactivation while the latter have been shown to compete with inactivation. In other respects, the actions of the two groups are very similar: both have access to their blocking site when the channel is open, and both simulate inactivation. We have studied the effects of two structurally similar three-ring compounds, 9AA and AzA, one with and one without use-dependence. We conclude that both compounds compete with inactivation. 9AA clears from the channels in two phases: the faster requiring milliseconds and the slower seconds. AzA has only the fast phase and thus no use-dependence. After removal of inactivation, 9AA has only the fast phase of clearing and has lost its use-dependence. Both 9AA and AzA slow the closing of Na channels. With both compounds, the tail currents are prolonged which could not occur if the channels were inactivated. Thus both compounds compete with inactivation. Mechanistically, we think that the activation gate can close without great difficulty on 9AA, trapping this agent and causing use-dependence. The gate cannot close on AzA, possibly because of its larger size. Gating current measurements confirm these ideas, in that 9AA immobilizes gating charge much less than AzA. Further evidence that inactivation of the channel is not essential for use-dependent block is that QX-314 still causes some use-dependence after removal of inactivation with pronase.

**M-AM-H12** MOLECULAR MOTION IN SODIUM CHANNELS by David Landowne

Dept. of Physiology and Biophysics, University of Miami School of Medicine, Miami, FL 33101

Almost coincident with the nerve action potential there is a change in the retardation (linear birefringence) of the squid giant axon by about 0.15 pm. This equivalent to about 150 peptide bonds per channel rotating 90° or a larger number rotating through a smaller angle.

During a step depolarization of the membrane, the birefringence change exhibits a rapid phase associated with activation of the sodium channel molecule and a slow phase associated with its inactivation. With pairs of pulses the amplitude of the rapid phase corresponds to the magnitude of the fast gating charge movement, both are reduced during immobilization or inactivation.

The rapid birefringence change precedes the opening of sodium channels. Thus there are three measurable transitions between four different states. There are voltage-dependent molecular motions associated with activation and inactivation and there is a voltage-dependent opening of the aqueous ionic pathway.

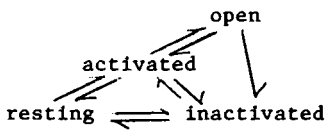


Supported by NIH DRR #S07 RR 05363 (BRSG)